SRNL-STI-2011-00026

Key Words:
Jet Mixing,
Turbulence Model

Retention:
Permanent

ADVANCED MIXING MODELS

R. A. Dimenna, S. Y. Lee, and D. A. Tamburello
Savannah River National Laboratory

FEBRUARY 2011

Savannah River National Laboratory
Savannah River Nuclear Solutions
Aiken, SC 29808

Prepared for the U.S. Department of Energy Under
Contract Number DE-AC09-08SR22470

DISCLAIMER

Printed in the United States of America

Prepared for
U.S. Department of Energy

SRNL-STI-2011-00026

Key Words:
Jet Mixing,
Turbulence Model

Retention:
Permanent

ADVANCED MIXING MODELS

R. A. Dimenna, S. Y. Lee, and D. A. Tamburello
Savannah River National Laboratory

FEBRUARY 2011

Savannah River National Laboratory
Savannah River Nuclear Solutions
Savannah River Site
Aiken, SC 29808

Prepared for the U.S. Department of Energy Under
Contract Number DE-AC09-08SR22470

REVIEWS AND APPROVALS

R. A. Dimenna, Co-author, Process Modeling & Comp. Chemistry Group Date

S. Y. Lee, Co-author, Applied Comp. Eng. & Statistics Group Date

D. A. Tamburello, Co-author, Applied Comp. Eng. & Statistics Group Date

M. A. Shadday, Peer Reviewer, Applied Comp. Eng. & Statistics Group Date

P. L. Lee, Manager, Applied Comp. Eng. & Statistics Group Date

S. J. Hensel, Manager, Computational Engineering and Sciences Date

TABLE OF CONTENTS

LIST OF FIGURES

LIST OF TABLES

NOMENCLATURE

A	Area
C	Concentarion or constant for equation
C_a	Constant used in Eq. (23)
C_{eq}	Equilbrium concentarion
C_o	Constant used in Eq. (1)
C_v	Constant in Eq. (18)
D	Tank diameter
D_m	Mass diffusion coefficient
d_o	Jet nozzle diameter
E	Kinetic energy
F	Correlation constant used in Table 2.
f_{jet}	Jet mixing time factor used in Table 2
g	Gravitational acceleration
h_l	Liquid heght
k	Turbulent kinetic energy per unit mass
k_v	Wave number at lower bound limit of viscous disspitation
k_w	Wave number used in Eq. (9)
L	Jet length or maximum integral length scale
M	Fluid momentum
m	Total mass flow rate
m_o	Mass flow rate at jet inlet
m_1	Entrained mass flow rate
p	Pressure
Δp	Pressure drop
Q	Volumetric flow rate
Q_j	Jet volumetric flow rate
R	Tank or pipe radius
Re_T	Taylor Reynolds number
r	Local radial distance of turbulent jet region
r_a	Local radius of turbulent jet flow boundary in Eq. (20)
T	Time interval used in Eq. (4)
t	Time
t_d	Kolmogorov time
t_m	Mixing time in Eq. (2)
U_o	Velocity at jet inlet
U	Local velocity along the jet discharge direction
u	Transient velocity or local velocity along the x-axis
u_i	Local velocity (i = 1 for x-axis, i = 2 for y-axis, i = 3 for z-axis)
u_i'	Turbulent fluctuating velocity (i = 1 for x-axis, i = 2 for y-axis, i = 3 for z-axis)
u_j	Local velocity (j = 1 for x-axis, j = 2 for y-axis, j = 3 for z-axis)
u_j'	Turbulent fluctuating velocity (j = 1 for x-axis, j = 2 for y-axis, j = 3 for z-axis)
u_x	Local velocity along the x-axis
u_y	Local velocity along the y-axis
< >	Time-averaging symbol for a parameter inside a sharp bracket
v(x)	Local velocity at a point x
v_{rms}	Root-mean-square velocity
x	Local distance along the x-axis

ε	Turbulent energy dissipation rate per unit mass
ε_v	Turbulent energy dissipation rate per unit volume
ρ	Fluid density
λ	Turbulent length scale
λ_B	Batchelor length scale
λ_d	Kolmogorov length scale
λ_{dif}	Diffusion length
μ_t	Turbulent dynamic viscosity (= $\rho \nu_t$)
ν	Kinematic viscosity
ν_t	Turbulent eddy diffusion coefficient
φ_v	Non-dimensional velocity distribution
Re	Reynolds number
Re_{jet}	Reynolds number based on jet operating conditions
SRS	Savannah River Site
CFD	Computational Fluid Dynamics
DNS	Direct Numerical Simulation
DOE	United States Department of Energy
DWPF	Defense Waste Processing Facility
ECR	Effective Cleaning Radius
EFRT	External Flowsheet Review Team
FLUENT	CFD software code
N-S	Navier-Stokes
PNNL	Pacific Northwest National Laboratory
RKE	Realizable k-ε
SMP	Slurry Mixer Pump
SMP	Submersible Mixer Pump
SRS	Savannah River Site
wt	weight

1.0 EXECUTIVE SUMMARY

The process of recovering and processing High Level Waste (HLW) the waste in storage tanks at the Savannah River Site (SRS) typically requires mixing the contents of the tank with one to four mixers (pumps) located within the tank. The typical criteria to establish a mixed condition in a tank are based on the number of pumps in operation and the time duration of operation. To ensure that a mixed condition is achieved, operating times are typically set conservatively long. This approach results in high operational costs because of the long mixing times and high maintenance and repair costs for the same reason. A significant reduction in both of these costs might be realized by reducing the required mixing time based on calculating a reliable indicator of mixing with a suitably validated computer code.

The focus of the present work is to establish mixing criteria applicable to miscible fluids, with an ultimate goal of addressing waste processing in HLW tanks at SRS and quantifying the mixing time required to suspend sludge particles with the submersible jet pump. A single-phase computational fluid dynamics (CFD) approach was taken for the analysis of jet flow patterns with an emphasis on the velocity decay and the turbulent flow evolution for the far-field region from the pump. Literature results for a turbulent jet flow are reviewed, since the decay of the axial jet velocity and the evolution of the jet flow patterns are important phenomena affecting sludge suspension and mixing operations.

The work described in this report suggests a basis for further development of the theory leading to the identified mixing indicators, with benchmark analyses demonstrating their consistency with widely accepted correlations. Although the indicators are somewhat generic in nature, they are applied to Savannah River Site (SRS) waste tanks to provide a better, physically based estimate of the required mixing time.

Waste storage tanks at SRS contain settled sludge which varies in height from zero to 10 ft. The sludge has been characterized and modeled as micron-sized solids, typically 1 to 5 microns, at weight fractions as high as 20 to 30 wt%, specific gravities to 1.4, and viscosities up to 64 cp during motion. The sludge is suspended and mixed through the use of submersible slurry jet pumps. To suspend settled sludge, water is added to the tank as a slurry medium and stirred with the jet pump. Although there is considerable technical literature on mixing and solid suspension in agitated tanks, very little literature has been published on jet mixing in a large-scale tank.

One of the main objectives in the waste processing is to provide feed of a uniform slurry composition at a certain weight percentage (e.g. typically ~13 wt% at SRS) over an extended period of time. In preparation of the sludge for slurrying, several important questions have been raised with regard to sludge suspension and mixing of the solid suspension in the bulk of the tank:

- How much time is required to prepare a slurry with a uniform solid composition?
- How long will it take to suspend and mix the sludge for uniform composition in any particular waste tank?
- What are good mixing indicators to answer the questions concerning sludge mixing stated above in a general fashion applicable to any waste tank / slurry pump geometry and fluid / sludge combination?

Grenville and Tilton (1996) investigated the mixing process by giving a pulse of tracer (electrolyte) through a submerged jet nozzle and by monitoring the conductivity at three locations within the cylindrical tank. They proposed that the mixing process was controlled by the turbulent kinetic energy dissipation rate in the region far away from the jet entrance. They took the energy dissipation rates in the regions remote from the nozzle to be proportional to jet velocity and jet diameter at that location. The reduction in the jet velocity was taken to be proportional to the nozzle velocity and distance from the nozzle. Based on their analysis, a correlation was proposed. The proposed correlation was shown to be valid over a wide range of Reynolds numbers (50,000 to 300,000) with a relative standard deviation of $\pm$ 11.83%.

An improved correlation including the effect of circulation time was proposed by Grenville & Tilton (1997) via a better fit of mixing time data for turbulent jet mixing under a wider range of jet Reynolds numbers (50,000 to 300,000). The circulation time was defined as the liquid volume divided by the entrained flow rate. They assumed that the mixing rate at the end of the jet length controls the mixing time for the entire tank by estimating the kinetic energy dissipation rate as discussed earlier. They predicted that for a given volume, an optimum geometry exists for a mixing vessel, allowing a desired mixing time to be achieved for a minimum power input. The current work compares their correlation of the jet mixing time with CFD modeling results for their experimental tanks in an attempt to achieve a fundamental understanding of the turbulent jet mixing and to establish mixing indicators.

The literature reviews on turbulent jet mixing analysis are summarized as follows:

- Jet flow evolution plays a significant role in jet mixing including jet nozzle orientation inside the tank, range of jet Reynolds numbers, and a recirculation effect coupled with the geometrical aspect ratio of liquid depth to tank diameter.
- Mixing time is dependent on Reynolds number and scale ratios. For mixing operations with high Reynolds number, the mixing time is primarily dependent on scale ratios.
- Mixing time for a large volume tank is not affected by the angle of nozzle inclination.
- Most literature results are limited to high depth of liquid above the jet location since no vortex formations were observed at the top liquid surface. Thus, the effect of Froude number referred to the nozzle under high tank liquid level was neglected in correlating the mixing time.

Turbulence parameters identified as potential indicators of mixing within a large tank were identified based on a two-equation turbulence closure model, the RKE model. The parameters selected were the turbulent kinetic energy, the turbulent kinetic energy dissipation rate, and especially the turbulence eddy viscosity. All three were calculated for tank mixing geometries and conditions documented by Grenville and Tilton (1996) and compared against the results of their correlation for mixing time. The fact that the results obtained with CFD calculations were qualitatively similar to those observed by Grenville and Tilton, even when the tank initial conditions differed, has lent insight into the influence of convective flow in tank mixing.

The concept of using the identified mixing indicators to characterize a mixing time was shown to have promise by investigating a range of computational variations including grid sensitivity, time step sensitivity, tank geometries, jet dimensions, and Reynolds number. In all cases, qualitatively similar results were obtained between the calculated flow patterns and the Grenville-Tilton correlation.

Based on the results of this work, recommendations for further investigation, including the development of the theory underlying the use of the mixing indicators, are as follows:

1. Define the observable parameters to be used as mixing indicators. This will include as part of the definition an evaluation of how those indicators should be observed in the computational output.
2. Identify the most applicable models to calculate the local turbulence parameters and their combinations such as the Taylor Reynolds number.
3. Characterize the impact of using special near-wall models for flow near walls and internal obstructions.
4. Evaluate the impact of using a rotating pump or pumps as the mixing driver on the calculation of the indicators.
5. Apply the results of the single phase analysis to the suspension of sludge particles in a waste tank.

While all parameters affecting the calculation of turbulent flow behavior in a vessel will be considered potential variables, two of the most significant ones are grid density and Reynolds number. Both of these will be addressed as key parameters in the mixing evaluation.

2.0 INTRODUCTION

2.1 Motivation

The process of recovering the waste in storage tanks at the Savannah River Site (SRS) typically requires mixing the contents of the tank to ensure uniformity of the discharge stream. Mixing is accomplished with one to four dual-nozzle jet mixers located within the tank. The jet mixers may be fixed in position or they may rotate depending on the specific mixing requirements.

The typical criteria to establish a mixed condition in a tank are based on the number of pumps in operation and the time duration of operation. To ensure that a mixed condition is achieved, operating times are set conservatively long. This approach results in high operational costs because of the long mixing times and high maintenance and repair costs for the same reason. A significant reduction in both of these costs might be realized by reducing the required mixing time based on calculating a reliable indicator of mixing with a suitably validated computer code.

The work described in this report establishes the basis for further development of the theory leading to identifying mixing indicators, the benchmark analyses demonstrating their consistency with widely accepted correlations, and an application of those indicators to SRS waste tanks to provide a better, physically based estimate of the required mixing time.

2.2 Background

Waste storage tanks at SRS consist of four types, Types I through IV, in terms of tank structure and capacity as illustrated in Fig. 1. The Type-I tank has about a 0.75-million gallon capacity with a 75-ft diameter; the others have 1- to1.3-million gallon capacities with an 85-ft diameter. Their heights range from 25 ft to 34 ft. They contain settled sludge which varies in height from zero to 10 ft. The sludge has been characterized and modeled as micron-sized solids, typically 1 to 5 microns, at undissolved solids concentrations, as high as 20 to 30 wt%, specific gravities to 1.4, and viscosities up to 64 cp during motion.

Settling rates of the sludge suspension vary inversely with the solids weight percent and have been reported to be on the order of 5 inches/hr at 1.5 wt% to 0.1 inch/hr at 13 wt%. The sludge is suspended and mixed through the use of submersible slurry jet pumps. To suspend settled sludge, water is added to the tank as a slurry medium and stirred with the jet pump.

A jet mixer pump has a bottom suction and two opposing discharge nozzles as shown in Fig. 2. Nozzle sizes range from 1.5 to 6 inches in diameter depending on the pump design. The nozzle discharge velocity is typically about 100 ft/sec. The pump is immersed in the sludge layer, allowing a recirculating mixture of sludge and water to serve as the feed flow. The discharge jet entrains waste as it expands into the tank and lifts sedimented waste, or sludge, from the tank bottom. Typically, several pumps can be inserted into the waste tanks through 0.57-m diameter openings and mounted to a rotating turntable located on the tank roof. Pump locations are typically different for every tank because of limited accessibility. Two types of the jet pumps have been typically employed for the mixing and solids suspension of the sludge at SRS. They are quad volute and standard slurry pumps. Their

jet flow is fully-developed turbulent under typical operating conditions since its Reynolds number has around 10^6 in terms of jet diameter and discharge velocity. Their designs and operating parameters are summarized and compared in Table 1. Both pump designs use a horizontal discharge, and the data in Table 1 provides an indication of the range of jet characteristics typical of the jet mixing to be evaluated as a result of the concepts developed in this project.

Although there is considerable technical literature on mixing and solid suspension in agitated tanks, very little literature has been published on jet mixing in a large-scale tank (Lee et al. 2008). Current guidelines to ensure a homogeneous feed to the Defense Waste Processing Facility (DWPF) from the waste storage tanks are set to conservatively long mixing times and lead to slurry mixer pump (SMP) failures as a result. If shorter mixing times can be shown to support DWPF or other feed requirements, longer SMP lifetimes can be achieved with associated operational cost and schedule savings. The ultimate goal of the present work is to demonstrate through computational methods and analysis that shorter SMP mixing times can meet DWPF feed composition acceptance requirements and other performance criteria, such as H_2 release requirements.

2.3 Methodology

Two aspects of mixing the contents of a waste tank containing settled sludge are:

1. Suspending the sludge that may have been settled in the tank for decades.
2. Mixing the suspended sludge once it has been entrained from the bottom of the tank.

Literature data (Lee et al. 2004, 2008) show that large particles are more easily eroded by streams than smaller ones. This phenomenon is more pronounced with small particles since the cohesive forces increase with decreasing size. The literature results show that for a given particle size, a certain velocity can be identified below which the particle will experience sedimentation, and a critical scour velocity, above which it will be eroded. Fluid velocities between these two values will transport solids of that size. The literature data (Lee et al. 2004) show that fluid velocity, particle size, specific gravity of particle, and tank liquid level are key parameters associated with particle suspension. It should be emphasized that the incipient velocity of erosion is actually dependent on the critical shear stress at which settled sediment begins to move. The critical shear stress of the cohesive sludge materials depends on the composition of the sludge material, the particle-size distribution, particle shape, and packing. A minimum fluid velocity for suspending cohesive sludge at SRS has been established and confirmed as 0.7 m/sec (2.27 ft/sec) (Lee et al. 2004). The previous work shows that this velocity, 0.7 m/sec, will erode the sludge layer for particle sizes larger than clay material (about 5 μm). Establishing this characteristic velocity for SRS sludge allows the local fluid velocity at any distance from the nozzle to be employed as a measure of the slurrying capability of the submersible jet.

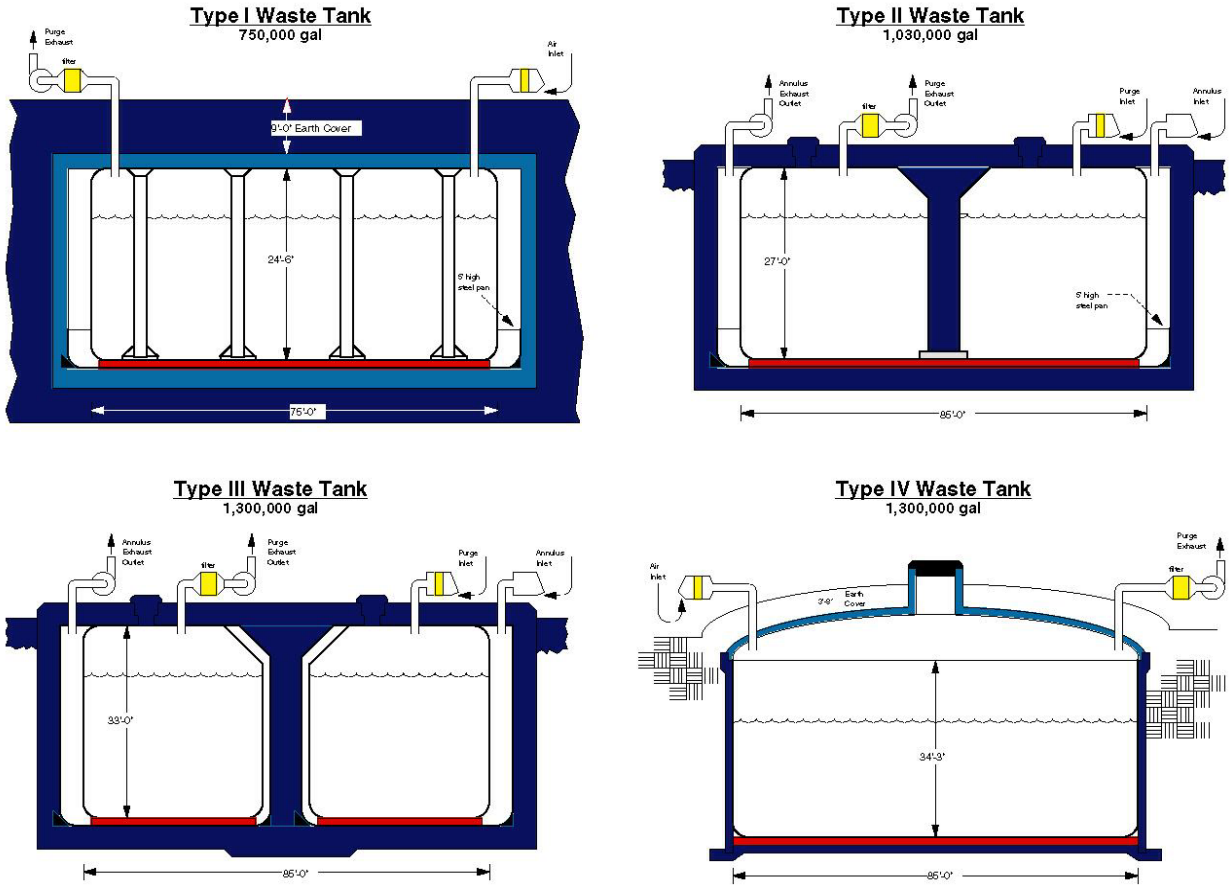

Figure 1. Four different types of high-level radioactive waste storage tanks at SRS

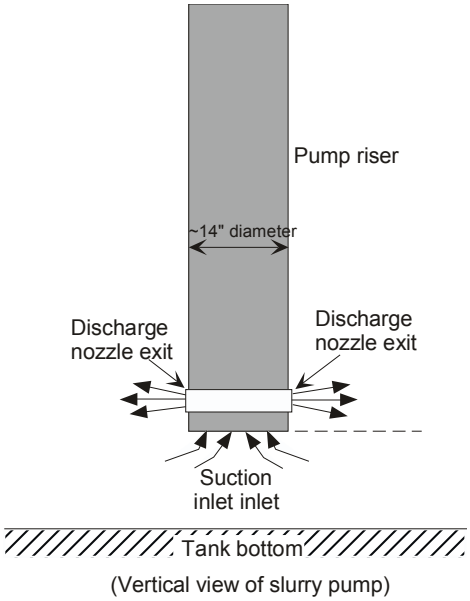

(Vertical view of slurry pump)

Figure 2. Schematic of a submersible pump with two opposing jets

Table 1. Pump design parameters for quad volute and standard slurry pumps used for jet mixing operations at SRS

Submersible jet pumps	Quad volute pump	Standard slurry pump*
Power, hp	300	150
Number of nozzles	2	2
Flow rate per nozzle, gpm	5200 gpm (2 nozzles)	1200 gpm (2 nozzles)
Nozzle diameter, inches	3.625	1.5
Pump operation mode	Indexed (or fixed position) or horizontal rotation	Indexed (or fixed position) or horizontal rotation
Pump rotation speed	0.2 to 0.25 rpm	0.2 to 0.25 rpm
Pump nozzle elevation above tank bottom, inches	About 12	About 12
Velocity at nozzle exit, ft/sec (m/sec)	80.8 (24.635)	109.0 (33.213)
Re_{jet}	2×10^6	1×10^6

Note:* Nominal operating conditions

The focus of the present work is on both aspects of tank mixing: to establish mixing criteria associated with the waste processing at SRS and to quantify the mixing time required to suspend sludge particles with the submersible jet pump. Prior to discussing the modeling approach, the literature results for a turbulent jet flow are reviewed briefly, since the decay of the axial jet velocity and the evolution of the jet flow patterns are important phenomena affecting sludge suspension and mixing operations.

The literature results (Abramovich 1963; Lee et al. 2004) show that when a turbulent jet of fluid is discharged from a nozzle into a stagnant fluid medium, it entrains fluid and expands. The fluid domain for a large-scale tank has both a solid wall boundary and a free surface boundary as the jet expands into the downstream region and ultimately recirculates via the suction on the bottom of the pump as shown in Fig. 2. The spreading fluid is retarded by the interaction with the wall as shown in Fig. 3, and the inner part of the flow may be expected to show a certain structural similarity to a boundary layer. Nonetheless, the typical jet nozzle elevation about the tank bottom is sufficiently high that the jet may be treated as a free jet (Davis & Winarto 1980). Entrainment of quiescent fluid occurs near the outer edges of the flow, and accordingly resembles a free jet (Abramovich 1963). In this case sludge particles near the edge of the jet plume are entrained into a turbulent zone, and they are suspended. Estimations of minimum suspension velocity, particle settling rate, and incipient erosion

velocity have been performed to support the use of a computational fluid dynamics (CFD) approach to establish and evaluate a sludge mixing criterion (Lee et al. 2008).

Most mixing action and entrainment takes place in the region of fully-developed flow which begins at a distance of approximately eight nozzle diameters from the exit plane (Abramovich 1963). From Abramovich (1963), when a turbulent jet of fluid is discharged from a nozzle with a diameter d_o into a quiescent fluid, the non-dimensional velocity distribution, φ_v, along the jet axis for a homogeneous fluid is approximated by

$$\varphi_v = \left(\frac{v(x)}{U_o}\right) = C_o\left[\frac{x}{d_o}\right]^{-1} \quad (1)$$

In Eq. (1), C_o is a constant determined by the turbulence characteristics of the jet, U_o the nozzle exit velocity, *v(x)* the local velocity at a point *x*, and *x* the distance from the nozzle. Abramovich (1963) correlated experimental data for a free turbulent jet submerged in fluid using the non-dimensional form provided by Eq. (1). From his work for a free jet without any flow obstructions, the proportionality constant C_o in Eq. (1) was determined to be 6.32.

In the free turbulent jet experiment, the only non-dimensional parameter is the jet's Reynolds number, Re_{jet}. The dependency of the following parameters on Re_{jet} needs to be examined:

- The self-similar velocity profile
- Velocity decay constant (C_o)
- The spreading rate (R_s) defined by $r_{1/2}(x)/(x - x_o)$

Mean flow profile and the spreading rate are independent of Re_{jet} as shown in Table 2. However, it is evident the Reynolds number does affect the flow in terms of turbulent characteristics such as local entrainment behavior. The virtual origin is denoted by x_o, and the local half-width of the jet by $r_{1/2}(x)$. In the self-similar region (x/d > 40 [Bradbury, 1965]) of high Reynolds number turbulent jets (Rejet > 10,000), the centerline velocity U_{max} and the half width $r_{1/2}$ are linearly proportional to the separation distance from the jet exit.

Since the pump discharge flow inside the large-scale tanks at SRS is affected by the bottom of the tank and internal flow recirculation, the constant C_o is evaluated from previous Tank 18 calculations rather than classical free jet theory. It was found to be 4.874 (Lee et al. 2004). The maximum axial velocity at any axial position *x* in an SRS waste tank can then be estimated using Eq. (1). The equation shows that the velocity at any point in the region of established flow is directly proportional to the product, d_oU_o. The axial entraining distance corresponding to the minimum entrainment velocity can be estimated with nozzle diameter and flow rate.

Table 2. Velocity decay constant and spread rate for free turbulent jets

Authors (year)	Re_{jet}	Decay constant (C_o)	Spreading rate (R_s)
Abramovich (1963)	20,000 - 4,000,000	6.31	---
Kiser (1963) (Conductivity cell data)	30,000	6.1	0.085
Rushton (1980)	5,600 – 200,000	$1.41Re_{jet}^{0.135}$	---
Panchapakesan & Lumley (1993)	11,000	6.06	0.096
Hussein et al. (1994) (Hot-wire data)	95,500	5.90	0.102
Hussein et al. (1994) (Laser-doppler data)	95,500	5.80	0.094

Fluid entrained in the jet region is transported and dispersed across it by motion induced from the largest to the smallest eddies. Eckart (1948) demonstrated that turbulent jet mixing can be viewed as a three-stage process of entrainment, dispersion (or stirring), and diffusion, spanning the full spectrum of space-time scales of the flow. In liquids, where species mass diffusivities are much smaller than kinematic viscosities resulting in a large Schmidt number (ratio of kinematic viscosity to mass diffusion coefficient), it is useful to split the diffusive action into two steps, one in which viscosity acts with acquisition of small-scale vorticity and the second where mass diffusion takes place. A mixed condition is reached at the time when the continuous liquid phase contains a spatially uniform composition of the discontinuous phase over the entire liquid domain of the tank. The current work focuses on the mechanical mixing related to the turbulent dispersion stirred by the jet entrainment, the principal driver for which is the convective flow the jet induces in the tank. A discussion on turbulent mixing will be provided later.

One of the main objectives in the waste processing is to provide the DWPF a uniform slurry composition at a certain weight percentage (typically ~13 wt%) over an extended period of time. In preparation of the sludge for slurrying to DWPF, several important questions have been raised with regard to sludge suspension and mixing of the solid suspension in the bulk of the tank:

- How much time is required to prepare a slurry with a uniform solid composition for DWPF?
- How long will it take to suspend and mix the sludge for uniform composition in any particular waste tank?
- What are good mixing indicators to answer the questions concerning sludge mixing stated above in a general fashion applicable to any waste tank / slurry pump geometry and fluid / sludge combination?

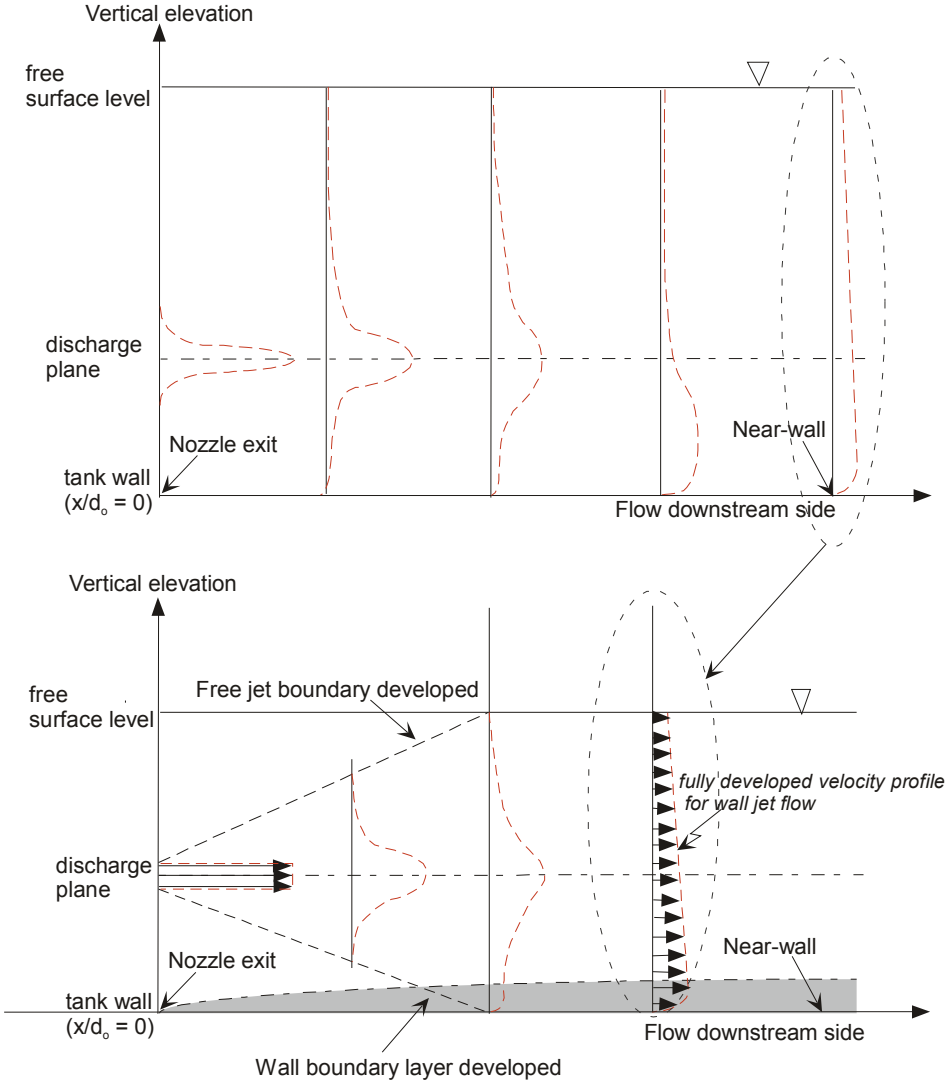

Figure 3. Typical velocity profiles in the direction perpendicular to the free surface from the previous modeling results of large-scale tank mixing simulations (Lee et al. 2008).

3.0 LITERATURE REVIEW ON JET MIXING STUDIES

3.1 General Review

Mixing is usually carried out to obtain a uniform mixture, and it can be achieved using mechanical agitators, fluid jet mixers, and static mixers or multiple T-junctions. This work is concerned with the mixing issues driven by a turbulent jet. In jet mixing, a fast stream of liquid is discharged into a stationary bulk liquid. The relative velocity between the jet region and the bulk liquid creates a turbulent mixing layer via the formation of turbulent eddies at the jet boundary as illustrated in Fig. 3. This mixing layer grows in the direction of the jet, entraining and mixing the jet liquid with the stagnant bulk liquid. Based on this concept, it has been assumed that longer jet lengths result in better mixing performance. The jet length, L, in the literature has been defined as the maximum distance a jet travels before it impinges on the opposite wall. For a cylindrical tank, the longest jet occurs when a jet is discharged at the bottom of the tank diagonally upward toward the opposite side. Thus, most researchers, including Grenville & Tilton (1996, 1997), have considered an inclined injection angle of about 45^{o} for their experimental investigations to quantify mixing performance and time.

Various techniques have been employed by researchers to examine the mixing behavior of a jet in an attempt to achieve a fundamental understanding of turbulent mixing. These include optical techniques and conductivity measurements. The experimental results for the mixed system have been proposed in the form of correlations to quantify the mixing time for a jet. These mixing correlations can be divided into two main categories. One is dependent on turbulence parameters such as turbulent kinetic energy, energy dissipation rate, and turbulent eddy viscosity, although they are not easily measurable or quantifiable. The other is dependent on measurable quantities such as tank geometrical dimensions and jet flow conditions. However, all of the literature correlations are basically related to two primary parameters, a geometrical length scale and the turbulent eddy viscosity.

Fossett & Prosser (1949) used a conductivity technique to measure mixing time for a turbulent jet. Their correlation contains tank diameter, jet diameter, and jet exit velocity. It is independent of the jet Reynolds number and does not include the effect of kinematic viscosity on the mixing time. It is applicable to the range of jet Reynolds numbers, 4,500 to 80,000. Many other researchers developed a similar correlation as shown in Table 2.

Fox & Gex (1956) indicated that mixing time is dependent on the jet Reynolds number. The Reynolds number is defined in terms of propeller diameter and speed. As jet flow is changed from laminar (Re = 300) to the turbulent flow regime (Re = 150,000), its dependence on the jet Reynolds number becomes weaker.

Lane & Rice (1982) investigated liquid jet mixing employing an inclined side entry jet. In their experimental study, conductivity measurements for tracer concentration were made at a monitoring point at any time to estimate the mixing time. They studied two designs for inclined side entry jet mixing, and they correlated their data to develop a general expression for mixing time in terms of measurable parameters such as jet velocity, tank dimensions, and fluid properties. They proposed a correlation for jet mixing time to predict the time required to achieve a 95% degree of mixing throughout the tank using an inclined jet located at the side entry near the tank bottom. For C_{eq} the equilibrium concentration and C the transient concentration at a monitoring point, the 95% mixing time t_m was defined by

$$t_m = \left| \frac{C - C_{eq}}{C} \right| < 0.5 \qquad (2)$$

Their correlation has a mixing time factor, *F*, and the factor is a function of the jet Reynolds number, which is similar to the friction factor associated with the momentum dissipation. It is noted that the F factor exhibits two different trends in the laminar and the turbulent regions as shown in Table 2. As discussed earlier, its dependence on jet Reynolds number is significant in the laminar region and weak in the turbulent regime.

A number of experimental studies have been carried out to investigate the flow patterns associated with jet mixing. Maruyama et al. (1982) reported mixing times for horizontal jets, inclined jets toward top free surface, and jets perpendicular to tank floor. In this case, the jet was located near the corner of tank floor. They proposed that the mixing time is a function of Reynolds number and jet length, but they emphasized the role of the flow patterns inside the tank on the mixing time behavior.

Perona et al. (1998) performed mixing experiments with water in two different scales of tanks. They are 2 ft in diameter by 10 ft in length (230 gallons) and 10 ft in diameter by 40 ft in length (25,000 gallons). The smaller one was about 1/6 linear scale of the actual storage tanks and was made of Plexiglas to permit flow visualization studies. Data were taken with a single jet placed about a quarter tank length from one end pointed horizontally towards the center of the tank. The jet nozzles were straight pieces of pipe, and their diameter and velocity were varied with this configuration. Jet diameters of 0.62, 0.87, and 1.61 inches were tested with the jet located 1.25 inches above the tank bottom for the two smaller diameters and 1.75 inches above the floor for the largest-diameter jet in each of the two tanks. Tests were also made with two-directional opposed jets along the same axis at this location and also at the center of the tank lengthwise. In all cases the jet was positioned close to the bottom of the tank, in the range of 1 to 4 jet diameters from the floor to the jet centerline. They measured jet mixing times for long horizontal tanks with length-to-diameter ratios of 4 and 5. Mixing times in the 230 gallon tank decreased from 1800 seconds to 300 seconds as the jet Reynolds number was increased from 15,000 to 130,000. With a single jet in the 25,000 gallon tank, mixing times decreased from 4500 to 840 seconds as the jet Reynolds number was increased from 80,000 to 311,000. For two-opposing jets of the same diameter and location, mixing times were not significantly different from those of the single jet at the same flow rate. At a given flow rate, mixing times were significantly lower with a 1.38-in double jet than with a 1.93-in double jet. They found that about 28 tank volumes must be recirculated through the entrained jet for good mixing with tanks of this configuration. Their empirical correlation for mixing time is shown in Table 3.

Grenville & Tilton (1996) investigated the mixing process by giving a pulse of tracer (electrolyte) through the jet nozzle and by monitoring the conductivity at three locations within the tank. They proposed that the mixing process was controlled by the turbulent kinetic energy dissipation rate in the region far away from the jet entrance. They took the energy dissipation rates in the regions remote from the nozzle to be proportional to jet velocity and jet diameter at that location. The reduction in the jet velocity was taken to be proportional to the nozzle velocity and distance from the nozzle. Based on this analysis, a correlation was proposed. The proposed correlation was shown to be valid over a wide range of Reynolds numbers with a relative standard deviation of $\pm$ 11.83%.

An improved correlation including the effect of circulation time was proposed by Grenville & Tilton (1997) via a better fit of mixing time data for turbulent jet mixing under a wider range of jet Reynolds numbers (50,000 to 300,000). The circulation time was defined as the liquid volume divided by the entrained flow rate. They assumed that the mixing rate at the end of the jet length controls the mixing time for the entire tank by estimating the kinetic energy dissipation rate as discussed earlier. They predicted that for a given volume, an optimum geometry exists for a mixing vessel, allowing a desired mixing time to be achieved for a minimum power input. This optimum condition occurs when the aspect ratio of the tank height to diameter is $1/\sqrt{2}$. The current work will compare the Grenville & Tilton (1997) correlation of the jet mixing time with CFD modeling results for their experimental tanks in an attempt to achieve a fundamental understanding of the turbulent jet mixing and to establish mixing indicators.

3.2 REVIEW SUMMARY

The literature review on the quantitative measurement and evaluation of flow entrainment by a jet stream and the time required to reach a certain degree of homogeneity has been performed to investigate key turbulent parameters for use as mixing performance indicators. The literature reviews on turbulent jet mixing analysis are summarized as follows:

- Jet flow evolution plays a significant role in jet mixing including jet nozzle orientation inside the tank, range of jet Reynolds numbers, and a recirculation effect coupled with the geometrical aspect ratio of liquid depth to tank diameter.
- Mixing time is dependent on Reynolds number and scale ratios. For mixing operations with high Reynolds number, the mixing time is primarily dependent on scale ratios.
- Mixing time for a large volume tank is not affected by the angle of nozzle inclination.
- Most literature results are limited to high depth of liquid above the jet location since no vortex formations were observed at the top liquid surface. Thus, the effect of Froude number referred to the nozzle was neglected in correlating the mixing time.

Table 3. Models and correlations for mixing time

Model	Authors	Mixing time	Validity
Empirical model	Grenville & Tilton (1996)	$3.0\left(\frac{L}{d_o}\right)^2\left(\frac{d_o}{U_o}\right)$	(50,000 < Re_{jet} < 300,000)
Empirical model including the effect of circulation time	Grenville & Tilton (1997)	$S\left(\frac{D^2}{U_o d_o}\right)\left(\frac{h_l}{L}\right)$, where S = 9.34 for θ > 15°, and S = 13.8 for θ < 15°.	(50,000 < Re_{jet} < 300,000) The parameter θ in their correlation is inclination angle of the jet nozzle and the horizontal.
Empirical model	Fossett & Prosser (1949)	$\frac{9.0D^2}{U_o d_o}$	(4,500 < Re_{jet} < 80,000)
Empirical model	Fox & Gex (1956)	$\frac{f_{jet} h_l^{0.5} D}{(U_o d_o)^{4/6} g^{1/6}}$ (f_{jet} = f (Re) for jet mixing)	(270 < Re_{jet} < 155,000)
Empirical model	Perona et al. (1998)	$C\left(\frac{V_T}{Q_j}\right)\left(\frac{d_o}{L}\right)$, where the constant C is about 28 from data.	Long horizontal tank for d_o = 0.6m, H = 3m, d = 16, 22, 41 mm (including two opposing horizontal jets)
Empirical model	Okita & Oyama (1963)	$5.5\left(\frac{h_l}{D}\right)^{0.5}\left(\frac{D}{d_o}\right)^2\left(\frac{d_o}{U_o}\right)$	Inclined side entry jet (5,000 < Re_{jet} < 100,000)
Empirical model	Lane & Rice (1982)	$F\left(\frac{h_l^{0.5} D}{(U_o d_o)^{0.667} g^{0.166}}\right)$, where F = $C_1(Re_{jet})^{-1.133}$ for laminar flow and $C_2(Re_{jet})^{-0.166}$ for turbulent flow	(200 < Re_{jet} < 100,000)
Dispersion model (G. I. Taylor)	Fischer (1973)	$C\left(\frac{\lambda^2}{\nu_t}\right)$	The constant C is dependent on flow conditions.
Eddy dissipation model	Spalding (1971)	$\left(\frac{k}{\varepsilon}\right)$	High Re (fully turbulent region)
Engulfment model	Baldyga & Bourne (1984)	$C\left(\frac{\nu_t}{\varepsilon}\right)^{0.5}$	High Re (fully turbulent region) The constant C is dependent on flow conditions.

4.0 BASIC CHARACTERISTICS OF TURBULENT FLOW MIXING AND ITS INDICATORS

A turbulent flow consists of high levels of fluctuating vorticity. At any instant, vortical motion, called eddies, are present in the flow. These eddies range in size from the largest geometric scales of the flow down to small scales where molecular diffusion dominates. The eddies are continuously evolving in time, and the superposition of their induced motions leads to fluctuating waves. Turbulent kinetic energy is passed from the largest eddies to the smallest though a process called the energy cascade. At the smallest scales, the energy is dissipated as heat by viscous effects. Thus, one of the basic characteristics of turbulent flow is dissipation of kinetic energy. To maintain turbulence, a constant supply of energy must be fed to the turbulent fluctuations at the largest scales from the mean motion.

The requirement of supplying energy to the turbulent fluctuations introduces the bulk convective motion into the mixing process. As will be discussed below, the dissipation of turbulent kinetic energy is a local phenomenon, whereas mixing is typically considered a global condition, even if it is realized and observed locally. For jet mixed tanks, the local dissipation of turbulent kinetic energy is fast compared to the convective distribution of the kinetic energy. The distribution of the energy is especially impacted when complex flow patterns develop, a point that has been addressed by Patwardhan & Joshi (1999) for impeller mixed tanks. This makes integral scale parameters such as vessel geometry and jet parameters significant when characterizing a mixing time. The coupled effects of Reynolds number, bulk convection, and flow patterns will be discussed in the sections to follow.

Understanding the turbulent energy dissipation process associated with solids or tracer mixing requires understanding the basic characteristics of turbulent flow. These characteristics include unpredictability, rapid diffusivity, high levels of varying vorticity, and dissipation of kinetic energy. For a stationary velocity record, the instantaneous velocity u can be decomposed into the sum of time-averaged and fluctuating components, which is called Reynolds decomposition.

$$u = < u > + u' \tag{3}$$

In this equation, <u> is the time-averaged quantity denoted as a sharp bracket, and u' is the fluctuating component corresponding to the deviation from the time-averaged value. The time-averaged fluctuating velocity is zero. Higher order statistical terms such as the variance are used as the magnitude of the fluctuations. For instance, the square root of the variance of the velocity fluctuations $\sqrt{< u'^2 >}$ is non-zero, and it is defined as the root-mean-square (rms) velocity and denoted as v_{rms}. When T is a time much longer than the longest turbulent fluctuations in the flow, v_{rms} is expressed as

$$v_{rms} = \sqrt{< u'^2 >} = \sqrt{\frac{1}{T}\int_0^T (u - < u >)^2 dt} \tag{4}$$

The velocity v_{rms} is used in quantifying the degree of local fluctuating velocity and is referred to as turbulent intensity in the literature (Hinze 1975).

4.1 Length Scales in Turbulent Flows

Motions in a turbulent flow exist over a wide range of length and time scales. The largest scales are limited by geometric dimensions such as pipe diameter or the depth of a large scale tank. These large scales are referred to as the integral length scales.

Experimental observations show that eddies lose most of their energy after one or two transits of the integral length scale. The rate of energy transferred from the largest eddies is proportional to their energy times their rotational frequency. The turbulent kinetic energy is proportional to the velocity squared, where the velocity is the fluctuating velocity characterized by the standard deviation. The rotational frequency is proportional to the rms velocity, v_{rms}, divided by the integral length scale L. From the Kolmogorov scaling law, the dissipation rate ε is of the order $(v_{rms})^3/L$ in the inertial regime of homogeneous isotropic turbulence before it reaches a scale where viscous dissipation becomes dominant. Following this formulation, Tennekes and Lumley (1972) estimated the dissipation length scale in terms of turbulent kinetic energy k and energy dissipation rate ε as

$$\lambda \approx k^{1.5}/\varepsilon . \tag{5}$$

It is noted that the rate of dissipation is independent of the fluid viscosity, and it is only dependent on the motion scale. However, the scale at which the energy dissipation occurs is strongly dependent on the fluid viscosity. Hence, the dissipation scale is estimated by combining the dissipation rate and the kinematic viscosity in an expression with dimensions of length, known as the Kolmogorov scale, λ_d.

$$\lambda_d \sim \left(\nu^3/\varepsilon\right)^{0.25} \tag{6}$$

Similarly, a time scale t_d and velocity scale v_d of the smallest eddies can be formed. They are

$$t_d \sim \left(\nu/\varepsilon\right)^{0.5} \text{ and } v_d \sim (\nu\varepsilon)^{0.25} \tag{7}$$

An analogous length scale can be estimated for the range at which molecular diffusion acts on a scalar quantity. This length scale is referred to as the Bachelor length scale, λ_B, and it is estimated as

$$\lambda_B \sim \left(\nu D_m^{\,2}/\varepsilon\right)^{0.25} \tag{8}$$

The ratio of the Kolmogorov to Bachelor length scales is equal to the square root of the Schmidt number, Sc. The Schmidt number is the ratio of kinematic viscosity, ν, to molecular diffusion coefficient, D_m.

Using SRS waste tank mixing as an example, the local suspension velocity is 0.01 m/sec and the integral length scale is roughly 6 inches corresponding to half of loose sludge layer. The fluid is water at room temperature with a kinematic viscosity of 10^{-6} m^2/sec. The

Kolmogorov length λ_d and time t_d scales are about 0.6 mm (= 0.024 in) and 0.4 seconds, respectively. When a diffusivity D_m = 10^{-9} m^2/sec for the chemical tracer is used, the Batchelor scale λ_B is about 0.02 mm, which is about 31 times smaller than the Kolmogorov scale. These results show that the molecular concentration field has a much finer structure than the velocity field.

4.2 Energy Cascade

Turbulence causes the formation of eddies of many different length scales which populate the energy spectrum. The energy spectrum characterizes the turbulent kinetic energy distribution as a function of length scale, indicating the amount of turbulent kinetic energy contained in a specific length scale. A fundamental parameter describing the turbulence is the energy dissipation rate. It defines the rate at which energy is generated at the larger scales, cascades through the inertial subrange, and is finally dissipated in the viscous subrange of the turbulent spectrum. Most of the kinetic energy of the turbulent motion is contained in the large length scales. The energy cascades from these large scale structures to smaller scale structures by an inertial and essentially inviscid mechanism. This process continues, creating smaller and smaller structures which produce a hierarchy of eddies. Eventually this process creates structures that are small enough that molecular diffusion becomes important and viscous dissipation of energy dominates. The scale at which this happens is known as the Kolmogorov length scale, λ_d.

Energy is introduced into the turbulent energy spectrum at the largest length scale, L, and cascades down to the smallest eddies, which are on the order of the Kolmogorov length λ_d. When the size of eddies is small enough, molecular diffusion, which smooths out the concentration gradients of the second phase, is invoked. These two length scales at the extremes of the energy cascade can differ by several orders of magnitude at high Reynolds numbers. In between there is a range with its own characteristic length λ that has formed at the expense of the energy of the large ones. These scales are very large compared with the λ_d, but still very small compared with the large scale of the flow. The range of length scales is then, $\lambda_d < \lambda < L$. When a turbulent jet mixer discharges fluid through a nozzle of diameter d_o, the turbulent wave number κ_w induced by the jet corresponds to its own characteristic length λ. The wave number κ_w of an eddy length scale λ is given by

$$\lambda = 2\pi / \kappa_w \quad . \tag{9}$$

A hypothesis of Kolmogorov was that at very high Reynolds numbers, the statistics of scales in the range $\lambda_d < \lambda < d_o$ are universally and uniquely determined by the scale λ and the rate of energy dissipation ε.

The large turbulent length scales in the flow dictate the rate of energy dissipation. These large length scales draw energy from the mean flow, then transfer the energy to successively smaller scales until it is dissipated at the Kolmogorov microscale. Thus, turbulent mixing transfers energy over the entire range of wave numbers, from the lowest value of κ_w to the maximum value of κ_w. Over the intermediate range of the wave numbers, say, less than κ_v, the viscous dissipation of energy is not important. This is called as the inertial range. Beyond κ_v the spectrum is affected by the diffusion process. This entire process is referred to as the energy cascade.

The energy distribution at the largest length scales is generally controlled by the flow geometry and mean flow velocity magnitude. The smallest length scales are many orders of magnitude smaller than the largest scales and hence are isotropic in nature. In between these two bounding scales, $\lambda_d < \lambda < L$, the spectrum is only a function of the length scale λ and the dissipation rate ε. Hence, the energy cascade spectrum depends on the dissipation rate because the largest length scales set the rate and the energy is transferred through this range. The dissipated energy will contribute to mixing a second component or tracer species into the continuous fluid medium. The large length scales have the most energy and the distribution in that range depends on the boundary conditions. The smallest scales have less energy by several orders of magnitude. As discussed in the previous section, the smallest scale is the Batchelor scale λ_B, more than an order of magnitude smaller than the Kolmogorov scale λ_d.

4.3 Turbulent Flow Evolution

Turbulent flows must satisfy conservation of mass and momentum. Thus, in principle, the incompressible continuity and Navier-Stokes equations can be solved for the instantaneous turbulent flow field via direct numerical simulation (DNS). The difficulty is that an enormous range of scales must be accounted for in the calculation. To accurately simulate the turbulent flow field, the calculation must span the largest geometric scales down to the Kolmogorov and Batchelor length scales as discussed earlier. Even with the fastest, largest modern supercomputers, such a calculation can be achieved only for simple geometries with small computational domains at low Reynolds numbers.

In most situations, engineers are satisfied with an accurate assessment of the time-averaged flow quantities. To derive the time-averaged flow equations, the instantaneous conservation equations are modified by substituting the Reynolds decomposition, such as representing the instantaneous local velocity by mean and fluctuating velocity components. This results in time averaged equations and a Reynolds stress tensor corresponding to the momentum transport due to the turbulent eddy fluctuations. While the evolution equations for the time-averaged quantities are valid, they can not be solved since several new unknown quantities are introduced, resulting in more unknowns than equations. This is the closure problem of turbulence (Tennekes & Lumley, 1972). One of the unknown important quantities is related to the addition of the gradient of $< u_i' u_j' >$ to the time-averaged momentum equation. It is related to the energy transport due to the turbulent fluctuations. This production term in the turbulence energy equation is identical to the loss to turbulence term in the balance equation for the kinetic energy of the mean motion.

The energy budget for mean kinetic energy indicates that the total change in kinetic energy of the mean flow results from the combined effects of transport, viscous dissipation and loss to turbulence. The mean flow feeds energy to the large turbulence scales as discussed earlier. Viscous dissipation is generally small for the mean flow since the mean velocity gradients are small. The transport terms represent the spatial movement of mean kinetic energy.

The loss to turbulence term in the mean kinetic energy balance is identical to the shear production term, $\rho < u_i' u_j' > \frac{\partial < u_i >}{\partial x_j}$, in the energy budget of turbulent kinetic energy (Hinze

1975). These terms correspond to kinetic energy transfer from the mean scales to the turbulent scales. In the balance equation of turbulent kinetic energy, the viscous dissipation is not small. The dissipation of turbulent kinetic energy $< u_i' u_j' >$ is an important characteristic of every turbulent flow as discussed in the previous section.

4.4 Mixing Mechanisms in Turbulent Flows

The current work is concerned with mechanical mixing related to the formation of a uniform composition when a large scale tank is stirred by a turbulent jet. The turbulent flows contain irregular motions over a wide range of length and time scales. Hence, the major question is how these motions contribute to mixing, resulting in patterns of turbulent jet dissipation and the composition decay of tracer components as a function of distance from the jet exit.

The turbulent energy dissipation term, $< u_i' u_j' >$, referred to as the apparent shear stress tensor in the literature, is an important characteristic of turbulent decay when a jet is injected into a stagnant fluid. The mixing length λ and the turbulent eddy viscosity ν_t depend on the relative magnitude of the turbulent shear stress and the mean velocity gradient (Kays & Crawford 1980). That is,

$$\lambda = \frac{\sqrt{\left|\left\langle u_i' u_j' \right\rangle\right|}}{\left(\frac{\partial < u_i >}{\partial x_i}\right)} = \sqrt{\frac{\nu_t}{\left(\frac{\partial < u_i >}{\partial x_i}\right)}} \qquad (10)$$

In Eq. (10) the integers, *i* and *j*, represent coordinate indices. For instance, when the integer *i* value is equal to 1, 2, or 3, it means *x-, y-,* or *z*-coordinate in a Cartesian coordinate system, respectively. The eddy viscosity ν_t in the equation, referred to as apparent viscosity in the literature, is dependent on Reynolds number, boundaries, and position in the fluid. In contrast, molecular viscosity is independent of Reynolds number and position in the fluid medium. It is a physical viscosity and a transport property of fluid. The eddy viscosity is estimated from spectral quantities of the turbulence data involving turbulent kinetic energy (*k*) and its dissipation rate (ε). As discussed in Section 4.1, the spectral information of the velocity fluctuations is used to estimate the length scale, which provides information on the eddy viscosity. The turbulent eddy viscosity is a primary measure of length scale for momentum dissipation, and it is responsible for most of the mixing, as discussed by Tennekes and Lumley (1972).

The turbulent mixing of two fluids or of a fluid and entrained solids to promote chemical reactions or a fluid-solid slurry is a common process in modern industry. Effective use of turbulence can increase interfacial contact of species present in the primary fluid. Fluid or solid entrained in a turbulent region is transported and dispersed across a vessel by motion initiated at the largest eddies and transferred to the smallest eddies, where molecular diffusion has the opportunity to act. At this smallest scale, the ability of a high Reynolds number turbulent flow to generate large interfacial area permits the mixing to proceed effectively. This work will focus on the turbulent mixing process over the inertial range, which is related to fluid dynamical scales of most flows of interest, and is referred to as stirring or suspension mixing. Therefore, the mixing scales considered here are much larger than the ones required to molecularly mix two fluids (Miller 1991).

Large scale tanks at Savannah River Site (SRS) are equipped with submersible mixer pumps (SMP) containing two opposed jets to stir the sludge that is settled on the tank floor. Most fluid regions stirred by the jets may have isotropic turbulence with large Reynolds numbers since the scale size of the fluid domain is much larger than that of the nozzle size. Shear at a solid wall is negligibly small so that the turbulence energy created by the jets is dissipated isotropically. Large eddies formed by a jetted fluid near the pump are not isotropic, but as the eddies are dissipated into the fluid domain, the smaller eddies formed by the dissipation process become independent of the original direction and magnitude of the jetted velocity and eventually become nearly isotropic. Larger eddies carry particles across the streamlines, and smaller eddies cause the particles to spread and disperse into the continuous fluid medium.

As shown in Fig. 4, surrounding fluid is entrained into a turbulent jet and mixed with quiescent bulk fluid via turbulent eddies at the boundary of the jet region. As a result of this, turbulent shear stress increases rapidly due to the sudden increase of the mean velocity gradient. Thus, the turbulent eddy viscosity can be used as a good indicator for bulk mixing.

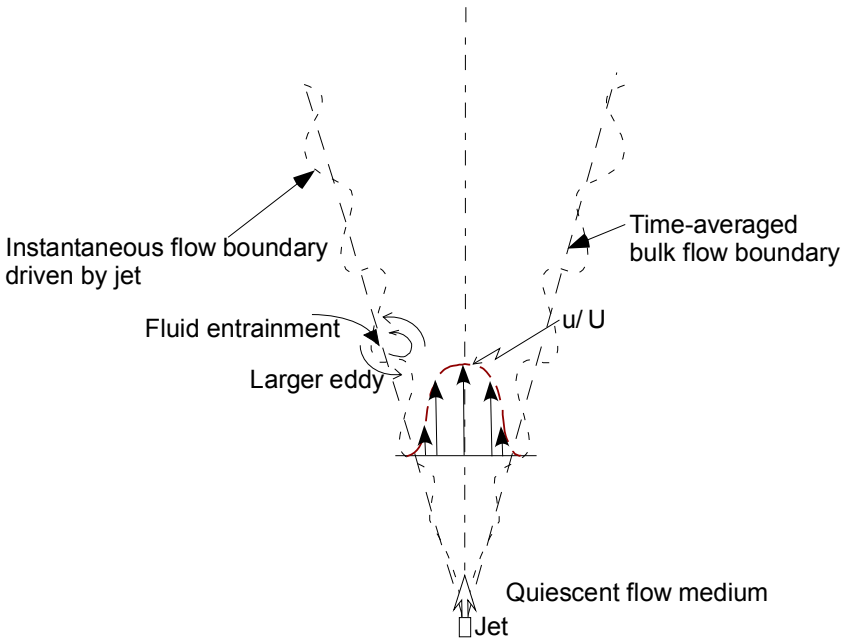

Figure 4. Schematic of fluid entrainment into a turbulent jet via the formation of turbulent eddies at the jet boundary

Most numerical models used to simulate turbulent mixing use time scales defined in terms of local isotropic properties. As shown in Table 3, most mixing times were determined by an empirical approach in terms of geometrical length scales and turbulent parameters. The mixing time is defined by a dissipation time scale for the energy containing eddies in the so-called inertial range. That is

$$t = \left(\frac{k}{\varepsilon} \right) \tag{11}$$

The kinetic energy per unit mass, k, is equal to $0.5v_{rms}^2$, where v_{rms} is defined in Eq. (4). The turbulent dissipation rate per unit mass ε can be estimated by the ratio of the power per unit volume involved in the mixing process. The power consumed by the process is given by the product of volumetric flow and pressure drop required for pumping flow. The pressure drop associated with the mixing flow requirement can be approximated with the Hagen-Poiseuille equation.

From the equations derived in the Appendix, turbulent energy dissipation rate per unit volume ε_v is calculated by Eq. (12).

$$\varepsilon_v \approx \left(\frac{Q\Delta p}{V}\right) = \left(\frac{Q\Delta p}{\pi R^2 L}\right) = 32\left(\frac{u}{D}\right)^2 \mu_t \tag{12}$$

All parameters used in Eq. (12) are defined in the Appendix. Turbulent energy dissipation rate per unit mass, ε, is associated with turbulent eddy viscosity.

$$\varepsilon = \frac{1}{\rho}\varepsilon_v = 32\left(\frac{u}{D}\right)^2 \nu_t \tag{13}$$

When combined with the kinetic energy $0.5u^2$ and turbulent energy dissipation rate given by Eq. (13), the mixing time t due to turbulent eddy dissipation is seen to be proportional to the square of a length scale, and inversely proportional to eddy viscosity.

$$t = C\left(\frac{D^2}{\left(\frac{\mu_t}{\rho}\right)}\right) = C\left(\frac{D^2}{\nu_t}\right) \tag{14}$$

The constant C in the above equation is a proportionality constant which can be determined by the literature data after a minimum value of eddy viscosity required for complete mixing is determined by Grenville and Tilton's correlation. Their empirical correlation for mixing time is consistent with the Equation (14) presented in terms of length scale and eddy viscosity.

In 1941, A. N. Kolmogorov introduced the idea that the smallest scales of turbulence are universal (similar for every turbulent flow) and that they depend only on ε and ν. The definitions of the Kolmogorov microscales can be obtained using this idea and dimensional analysis. Since the dimension of kinematic viscosity is length^2/time, and the dimension of the energy dissipation rate per unit mass is length^2/time^3, the only combination that has the dimension of time is $t_d = \left(\nu/\varepsilon\right)^{0.5}$ which is the Kolmorogov time scale. Similarly, the Kolmogorov length scale is the only combination of ε and ν that has dimensions of length.

The Kolmogorov (1941) theory is a mean field theory since it assumes that the relevant dynamical parameter is the mean energy dissipation rate. In fluid turbulence, the energy dissipation rate fluctuates in space and time, so it is possible to think of the microscales as quantities that also vary in space and time. However, standard practice is to use mean field values since they represent the typical values of the smallest scales in a given flow.

Theoretical analysis and experimental studies of mixing processes will result in an increased understanding of the mechanics that may lead to the development of improved mixing

devices or mixing indicators. For instance, suppose the order of magnitude of the mixing time that can be achieved is examined. The diffusion length λ_{dif} is given by ~$\sqrt{D_m t}$ where D_m is the diffusion coefficient and t is the mixing time. The length scale, λ_d, of the smallest eddies is given by Kolmogorov (1941) as given by Eq. (6). In his equation, ν is the kinematic viscosity and ε is the rate of dissipation of turbulent energy per unit mass. An efficient mixing device will dissipate a substantial fraction of the turbulent energy in the mixing time, so ε is roughly related to E/t where E is the initial energy of the turbulence. E is basically u^2. Sufficient mixing requires that the order of magnitude of λ_d be at least as small as that of λ_{dif}, so the minimum order of magnitude of the mixing time is found by equating λ_d to λ_{dif}. That is

$$t \approx \left(\frac{\nu^3}{(D_m u)^2} \right) = \left(\frac{D_m}{u^2} \right) Sc^3 \qquad (15)$$

An example of a turbulent mixing layer is illustrated diagrammatically in Fig. 4. It is assumed that a uniform irrotational stream emerges from a nozzle into a region where the surrounding fluid is at rest at atmospheric pressure. A sheet of vorticity will be generated at the interface between the moving fluid and the stationary fluid and this leads to the formation of a wedge-shaped turbulent mixing layer. It is observed experimentally that the turbulent mixing layer spreads outwards at a relatively small angle as indicated in the diagram, although it should be noted that the edges of the turbulent zone are intermittent in character like the outer edge of a turbulent boundary layer (Forstall & Shapiro 1950). When the turbulent boundary layer equation is applied to the mixing layer along the x-direction of the primary water flow as shown in Fig. 5, and the pressure gradient in the x-direction is assumed to be zero, the steady-state momentum conservation equation for the boundary mixing region in the x-direction is given as

$$\rho \left(\overline{u_x} \frac{\partial \overline{u_x}}{\partial x} + \overline{u_y} \frac{\partial \overline{u_x}}{\partial y} \right) \approx -\rho \left(\frac{\partial \left(\overline{u_x' u_y'} \right)}{\partial y} \right) \qquad (16)$$

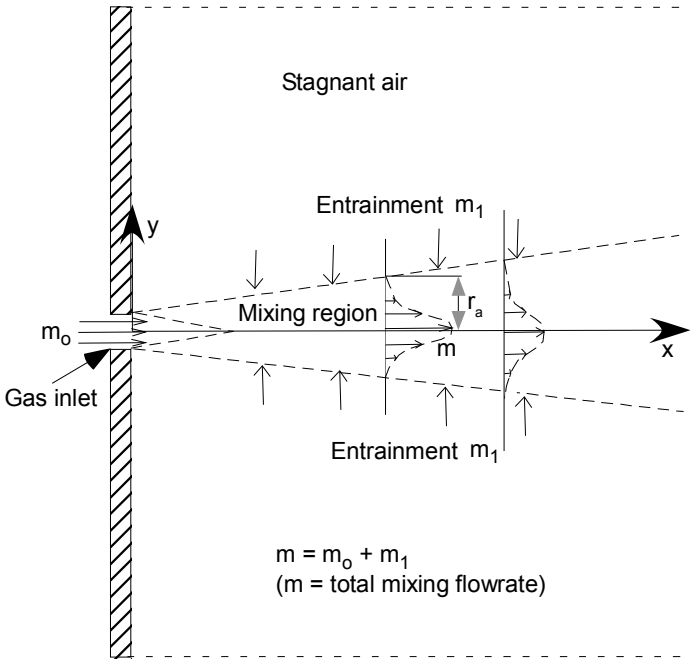

Figure 5. Water entrainment due to turbulent diffusion in three-dimensional turbulent jet under steady-state flow conditions

Following the literature approach (Kays & Crawford 1980) regarding the Reynolds stress term on the right-hand side of Eq. (16), it is reasonably assumed that the kinematic eddy viscosity ν_t should be constant with respect to *y* over the cross-section of the mixing layer. Using this assumption and the basic hypothesis of the turbulent mixing length, λ, the right-hand side term of the equation can be given in terms of the kinematic eddy viscosity ν_t, that is,

$$\left(\overline{u_x' u_y'}\right) = -\lambda^2 \left|\frac{\partial \overline{u_x}}{\partial y}\right| \left(\frac{\partial \overline{u_x}}{\partial y}\right) = -\upsilon_t \left(\frac{\partial \overline{u_x}}{\partial y}\right) \tag{17}$$

In Eq. (18) turbulent diffusivity is described by the center-line velocity *U* at distance *x*, assuming that the eddy viscosity is proportional to the thickness of the mixing layer multiplied by the overall velocity difference *U*.

$$\upsilon_t = C_\upsilon U x \tag{18}$$

From Eqs. (16) and (17), the resulting equation becomes

$$\left(\overline{u_x}\frac{\partial \overline{u_x}}{\partial x} + \overline{u_y}\frac{\partial \overline{u_x}}{\partial y}\right) \approx \upsilon_t \left(\frac{\partial^2 \overline{u_x}}{\partial^2 y}\right) \tag{19}$$

From Eq. (19), the flow momentum driven by the jet is dissipated by turbulent eddy diffusivity, ν_t, leading to the entrainment of the stagnant fluid into the water core region. Thus, the core region will eventually disappear because of the turbulent diffusion. During the turbulent diffusion process, the fluid momentum *M* should be conserved along the bulk

flow direction. When U is local maximum velocity at any distance x from the fluid inlet, the momentum at x becomes

$$M = 2\pi\rho(r_a)^2U^2\int_0^1\left(\frac{\overline{u_x}}{U}\right)^2\left(\frac{r}{r_a}\right)d\left(\frac{r}{r_a}\right) = \text{constant} \quad (20)$$

Hence, for a self-preserving flow pattern with profile similarity, Eq. (20) becomes

$$Ur_a = Ux = \text{constant} \quad (21)$$

The total flow rate m at local distance x is given by

$$m = 2\pi\rho(r_a)^2U\int_0^1\left(\frac{\overline{u_x}}{U}\right)\left(\frac{r}{r_a}\right)d\left(\frac{r}{r_a}\right) \quad (22)$$

When Eq. (21) is substituted for the local maximum velocity U under a self-preserving velocity profile, Eq. (22) becomes

$$m = m_o + m_1 = C_o r_a = C_1 x \sim \frac{C\upsilon_t}{U} \quad (23)$$

In Eq. (23) m_o and m_1 are flowrate at the inlet and total entrainment flow, respectively. The equation shows that the total mass flowrate increases linearly with respect to the discharge distance x of jet because of turbulent eddy viscosity at the edge of the boundary layer. This is consistent with test results (Ricou & Spalding 1961). As demonstrated by this example, turbulence dissipation due to eddies takes place in the downstream region of jet for large Reynolds number flow. During the momentum decay of the free jet, isotropic turbulent eddies occur since for a large-scale tank there is a large distance from a solid wall.

The viscous shear of an incompressible fluid flow near a solid wall results in the formation of vortex eddies. However, eddies formed by the motion of a solid object such as mechanical impeller are large, and they are not isotropic. As these eddies in a large scale tank decay, they transfer energy to smaller fluid fragments creating smaller eddies. These smaller generated eddies become independent of the solid bounding. The smaller eddies are considered isotropic, that is, they depend only on the power supplied and on the viscous dissipation. The present work will focus on the mixing evolved by isotropic turbulence.

Most mixing correlations developed by measured data have combinations of physical parameters such as jet diameter, jet velocity, tank diameter, and liquid viscosity as shown in Table 2. They all indicate that the most important parameter to determine mixing time is the momentum flux added to the tank (Fox & Gex 1956). They observed a clear effect of the jet Reynolds number on the mixing time except for high Reynolds numbers (larger than 4,500). Mixing time is a strong function of Reynolds number in the laminar jet regime, but only a weak function in the turbulent regime.

4.5 Review of Standard Two-Equation Turbulence (k-ε) Model

The *k*-ε model used for the present analysis is a two-equation model. In this model, transport equations are solved for two turbulence quantities, *k* and ε. These two modeling parameters need to be investigated in more detail.

The budget of turbulent kinetic energy (*k*)

Turbulence kinetic energy (*k*) is the mean kinetic energy per unit mass associated with eddies in turbulent flow. Physically, the turbulence kinetic energy is characterised by measured root-mean-square (rms) velocity fluctuations.

In the Reynolds-averaged Navier Stokes equations, the turbulence kinetic energy can be calculated based on the closure method, i.e. a turbulence model. Generally, the turbulent kinetic energy can be quantified by the mean of the turbulence normal stresses:

$$k = \frac{1}{2}\left\{\overline{(u_1)^2} + \overline{(u_2)^2} + \overline{(u_3)^2}\right\} \tag{24}$$

k can be produced by fluid shear, friction or buoyancy, or through external forcing at low-frequency eddie scales (integral scale). Turbulence kinetic energy is then transferred down the turbulence energy cascade, and is dissipated by viscous forces at the Kolmogorov scale. This process of production, convective transport and dissipation as modeled for *k* transport balance in the two-equation turbulence model can be expressed as:

$$\frac{Dk}{Dt} + \nabla \bullet T' = P - \varepsilon \tag{25}$$

where *Dk* / *Dt* is the mean-flow convection of *k*, *T'* the turbulent transport, *P* the production of *k*, and *ε* is the turbulent kinetic energy dissipation rate. The action of the mean velocity gradients working against the Reynolds stresses removes the kinetic energy from the mean flow and transfers it to the fluctuating velocity field as energy production term *P*.

$$T' = \frac{1}{2}\overline{(u_i u_j u_j)} + \frac{1}{\rho}\overline{(u_i p')} - \left(\frac{\mu}{\rho}\right)\overline{\left(u_j \frac{\partial u_i}{\partial x_j} + u_j \frac{\partial u_j}{\partial x_i}\right)} \tag{26}$$

$$P = -\overline{(u_i u_j)}\left(\frac{\partial \overline{U_i}}{\partial x_j}\right) \tag{27}$$

$$\varepsilon = \frac{1}{2}\left(\frac{\mu}{\rho}\right)\overline{\left(\frac{\partial u_i}{\partial x_j} + \frac{\partial u_j}{\partial x_i}\right)^2} \tag{28}$$

The resulting equation for *k* transport equation for incompressible turbulent flow is

$$\frac{Dk}{Dt} + \frac{\partial}{\partial x_i}\left\{\frac{1}{2}\overline{(u_i u_j u_j)} + \frac{1}{\rho}\overline{(p' u_i)}\right\} = \frac{\mu}{\rho}\nabla^2 k + P - \varepsilon \tag{29}$$

p' in Eq. (29) is fluctuating pressure.

Energy dissipation rate (ε)

A quantity of fundamental interest in turbulence is the dissipation field. In high Reynolds number flows, the viscous dissipation takes place at the smallest scales of motion. Due to

the isotropic assumption (loss of directional information) during the energy cascade to the smaller scales, the turbulence may be approxinmated as locally isotropic, in which case the dissipation term can be simplified to [Hinze, 1975]

$$\varepsilon(x) = K\upsilon_T \left\{ \frac{du(x)}{dx} \right\}^2 \tag{30}$$

K is a prefactor to be chosen to define averaged ε equal to its usual value for a three-dimensional isotropic field. The constant K is 15. The required fluctuating spatial derivative can be obtained from the temporal derivative of u' by invoking Taylor's frozen field approximation. That is, the velocity gradient term is equal to (u'/λ_g), where λ_g is called Taylor's microlength scale. υ_T is an arbitrary constant with units of eddy viscosity. In the fully turbulent region, measurements have been correlated by Eq. (31) [Baldyga et al., 1995].

$$\varepsilon = K' \left(\frac{U_{jet}{}^3}{d} \right) \left\{ \frac{(x - x_o)}{d} \right\}^{-4} \tag{31}$$

K' value was determined by experimental data, which was 48 [Antonia et al., 1994]. d is jet diameter. It is noted that kinetic dissipation rate decreases rapidly with the axial distance from the jet exit. Figure 6 shows some values of key turbulence parameters along the axial direction. Taylor's length scale λ_g grows linearly along the jet direction, which was correlated by Friehe et al. [1972].

$$\lambda_g = 1.07 \left(\frac{x}{\mathrm{Re}^{0.5}} \right) \tag{32}$$

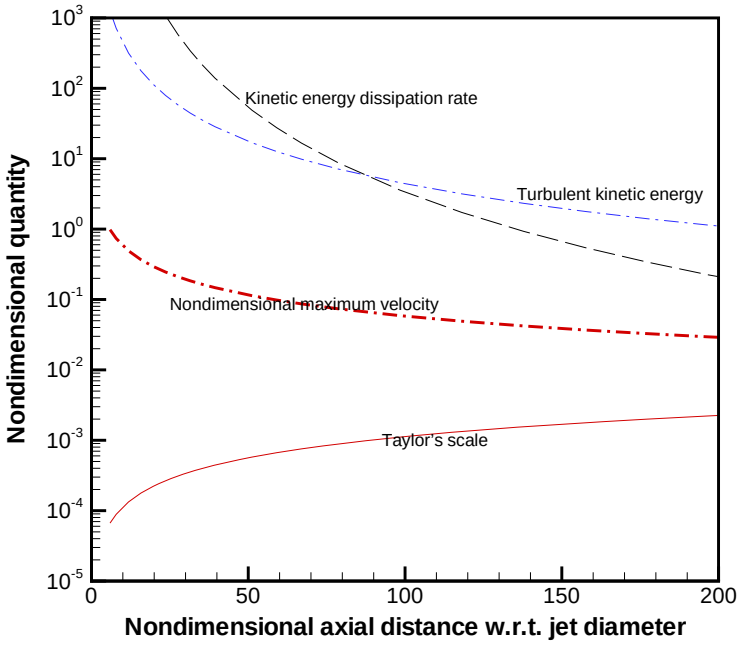

Figure 6. Axial distributions of convection velocity, turbulent kinetic energy, dissipation rate, Talyor's length scale based on Hussein et al.'s self-similar jet data

Characteristic Length Scale in k-ε Model

Flows at high Reynolds numbers are characterized by the existence of several length scales. In turbulent flows a wide range of length scales exist, bounded by the dimensions of the flow field as the upper limit and bounded by the diffusive action of molecular viscosity as the lower limit. Let's look at the steady state Navier-Stokes equation for incompressible fluid with constant viscosity.

$$u_j \bullet (\nabla u_i) = -\frac{1}{\rho}(\nabla P) + \upsilon \nabla^2 u_i \qquad (33)$$

The left-hand-side term, inertia, of Eq. (33) is scaled as U^2/L when U and L are assumed to be characteristic velocity and length scale. The second term, viscous diffusion, in the equation is represented by $\nu U/L^2$. The ratio of these two terms is UL/ν, the Reynolds number (Re). When a length scale λ is chosen such that the viscous terms are of the same order of the inertia magnitude for high Re number, the resulting equation becomes

$$\frac{U^2}{L} \approx \frac{\upsilon U}{\lambda^2} \qquad (34)$$

From Eq.(34) the ratio of the inertia to viscous diffusion length scales becomes

$$\frac{\lambda}{L} \approx \left(\frac{\upsilon}{UL}\right)^{0.5} = \mathrm{Re}^{-0.5} \qquad (35)$$

The viscous length scale λ is a transverse length scale. It represents the molecular diffusion due to the momentum difference across the flow, away from the surface. The diffusion length scale along the flow is negligibly small compared to the downstream transport of momentum by the bulk flow. This length scale may be associated with Taylor's micro-length scale.

The equation governing the mean kinetic energy $0.5\overline{(u_i u_i)}$ of the turbulent velocity fluctuations is obtained by multiplying the Navier-Stokes equations by u_i, taking the time average of all terms, and subtracting the kinetic energy balance equation of the mean bulk flow U_i. When a turbulent flow is maintained in a steady, homogeneous, pure shear flow, the resulting equation is reduced to the balance equation of the rate of turbulent energy production by Reynolds stresses and the rate of turbulent energy dissipation due to the flow fluctuations. The actions of the mean velocity gradients working against the Reynolds stresses remove the kinetic energy from the mean flow and transfers it to the fluctuating velocity field as the energy production term. That is,

$$-\overline{(u_i u_j)}\left(\frac{\partial U_i}{\partial x_j}\right) = \overline{\tau_{ij}\left(\frac{\partial u_i}{\rho \partial x_j}\right)} \tag{36}$$

where $\tau_{ij} = -\mu\left(\partial u_i \big/ \partial x_j\right)$.

From the turbulent energy budget in isotropic turbulence, the time-averaged viscous dissipation rate per unit mass in Eq. (36) is equal to

$$\varepsilon = \overline{\left(\tau_{ij}\frac{\partial u_i}{\rho \partial x_j}\right)} = K\left(\frac{\mu}{\rho}\right)\overline{\left(\frac{\partial u_i}{\partial x_i}\right)^2} \tag{37}$$

When the length scale λ_g is defined as the Taylor microscale in isotropic turbulence, Eq. (37) becomes

$$\varepsilon = K\left(\frac{\mu}{\rho}\right)\overline{\left(\frac{\partial u_i}{\partial x_i}\right)^2} = K\left(\frac{\mu}{\rho}\right)\left(\frac{u}{\lambda_g}\right)^2 \tag{38}$$

The RHS term in Eq. (36) is the deformation work due to turbulent stresses, known as turbulent energy dissipation. When Reynolds stress $\left(\frac{\partial U_i}{\partial x_j}\right)$ is of order (u/L), the LHS term in the equation is equal to (u^3/L). Then, from Eqs. (36) and (38), the Taylor microscale λ_g is expressed in terms of large eddy scale L.

$$\lambda_g = \sqrt{K}L\left(\frac{\mu}{\rho L u}\right)^{0.5} = \sqrt{K}L\,\mathrm{Re}^{-0.5} \tag{39}$$

In Eq. (39) K is a constant related to the bookkeeping from the square of the summation of the fluctuating velocity component gradients. When it is in the rage of 1.1 to 15 in the literature, it is noted that the Taylor microlength λ_g is much larger than the viscous diffusion

length λ in Eq. (35) for a given large-eddy scale Reynolds number. As shown in Eq. (38), λ_g may be regarded as a measure of the length scale of the dissipative eddies which are responsible for the dissipation of energy. In this respect, the Taylor' microscale is closely related to the local loss of the turbulent energy production, which contributes to local mixing.

With the turbulent viscosity υ_T written as

$$\left(\frac{\mu}{\rho}\right)_T = \lambda_m u^* \tag{40}$$

in the Prandtl mixing-length model, the lengthscale for simple shear flow is

$$u^* = \lambda_m \left|\frac{\partial \overline{U_i}}{\partial x_j}\right| \tag{41}$$

The implication is that the velocity scale is locally determined by the average velocity gradient. When the velocity gradient in Eq. (41) is zero, u* is zero and the mixing length is zero. Although there are several circumstances in which the velocity gradient is zero, the turbulent velocity scale can not be zero. As shown for the experimental results of the axisymmetric jet, direct measurement for turbulent viscosity is shown to be far from zero. Thus, Kolmogorov (1942) suggested that it is better to base the velocity scale on the turbulent kinetic energy, that is,

$$u^* = Ck^{0.5} \tag{42}$$

where C is a proportional constant.

From Eqs. (40) and (42), the turbulent viscosity becomes

$$\upsilon_T = Ck^{0.5}\lambda_m \tag{43}$$

In order for turbulent viscosity to be quantified, turbulent kinetic energy must be estimated by solving a transport equation for turbulence kinetic energy *k*. This is known as a one-equation turbulence model since a model transport equation is solved for one turbulence parameter *k* for a specified mixing length λ_m. As discussed earlier (RHS of Eq. (36)), at high Reynolds number the dissipation rate ε scales as u_c^3/λ_m, where u_c and λ_m are velocity scale and lengthscale of the energy-containing eddy motions. Thus, the resulting equation for ε becomes

$$\varepsilon = C^3 \frac{k^{1.5}}{\lambda_m} \tag{44}$$

From Eq. (44) the mixing length can be estimated for given *k* and ε values as

$$\lambda_m = C^3 \frac{k^{1.5}}{\varepsilon} \tag{45}$$

Based on the log-law region, *C* can be estimated for the shear flow of wall bounded flow as discussed later. The length scale λ_m is called the Prandtl mixing length in this document.

For isotropic turbulence flow at high Reynolds number, when k and ε are estimated from two-equation turbulence model, mixing lengthscale can be estimated by Eq. (45).

Governing Equations in k-ε Turbulence Model

From these two key parameters of k and ε, a lengthscale ($k^{1.5}/\varepsilon$), a timescale (k/ε), a quantity of turbulent eddy diffusivity (k^2/ε), can be formed without specification of flow-dependent mixing lengthscale λ [Jones and Launder, 1972]. When turbulent energy transport term T' in Eq. (26) is modeled with a gradient-diffusion hypothesis as

$$T' = -\frac{\upsilon_T}{\sigma_k}\nabla k \tag{46}$$

where the turbulent Prandtl number for kinetic energy is generally taken to be $\sigma_k = 1.0$. This equation assumes that there is a flux of k down the gradient of k due to velocity and pressure fluctuations. In summary, the transport equation for turbulent kinetic energy k is

$$\frac{Dk}{Dt} = \nabla \bullet \left(\frac{\upsilon_T}{\sigma_k}\nabla k\right) + P - \varepsilon \tag{47}$$

The three other terms, $-Dk/Dt$, P, and ε, are in closed form given the turbulent-viscosity hypothesis.

Turbulence consists of high levels of fluctuating vorticity. At any instant, vortical motion called eddies are present in the flow. These eddies range in size from the largest geometrical scales of the flow such as tank diameter down to small eddies where molecular diffusion dominates. The eddies are continuously evolving, and the superposition of their induced motions leads to the fluctuating waves. In this situation, turbulent kinetic energy is dissipated from the largest eddies down to the smallest through a process called energy cascade. In order to maintain the turbulence, a constant supply of energy must be fed to the turbulent fluctuations at the largest scales from the mean motions, where it is driven by a jet pump or mechanical agitator. Thus, turbulent energy dissipation rate ε is viewed as the energy-flow rate in the cascade, and it is determined by the large-scale motions, independent of the viscosity at high Reynolds number. Consequently, the transport equation for ε is best considered as being entirely empirical. That is,

$$\frac{D\varepsilon}{Dt} = \nabla \bullet \left(\frac{\upsilon_T}{\sigma_\varepsilon}\nabla \varepsilon\right) + C_1\left(\frac{\varepsilon}{k}\right)P - C_2\frac{\varepsilon^2}{k} \tag{48}$$

where the turbulent viscosity is

$$\upsilon_T = C_\mu \frac{k^2}{\varepsilon} \tag{49}$$

where $C_\mu = 0.09$.

From the Prandtl mixing length theory,

$$\left(\overline{uv}\right) = -\lambda_m{}^2\left(\frac{\partial \overline{U}}{\partial y}\right)^2 = -\left(u^*\right)^2 \tag{50}$$

From the literature results for the log-law function [Kim et al., 1987],

$$\left(\overline{uv}\right) \approx -0.3k \tag{51}$$

From Eqs. (50) and (51), mixing velocity becomes

$$u^* \approx \sqrt{0.3}\sqrt{k} = 0.55\sqrt{k} \tag{52}$$

It is consistent with Eq. (52) and C is equal to 0.55.

The turbulent viscosity for the mixing,

$$\left(\upsilon_T\right) = \lambda_m u^* \tag{53}$$

From Eqs. (45) and (52), Eq. (53) becomes

$$\upsilon_T = 0.55^4 \frac{k^2}{\varepsilon} \approx 0.09 \frac{k^2}{\varepsilon} = C_\mu \frac{k^2}{\varepsilon} \tag{54}$$

It is noted that the turbulent viscosity coefficient C_μ of 0.09 in the two-equation model (Eq. (49)) can be derived under the log-law. From these results, the two-equation turbulence model is good for the bulk model including the log-law shear region, but it will not be good for the flow within the laminar sublayer close to the wall as shown in the previous work [SRNL, 2008].

For an understanding of the ε equation, homogeneous turbulence is examined by using the two-equation k-ε model. The transient transport equations of ε and k, given in Eqs. (24) and (25), become

$$\frac{dk}{dt} = P - \varepsilon \tag{55}$$

$$\frac{d\varepsilon}{dt} = C_1\left(\frac{\varepsilon}{k}\right)P - C_2 \frac{\varepsilon^2}{k} \tag{56}$$

From Eq. (36), the production term P is zero in the absence of mean velocity gradients, and the turbulence energy decays. In this situation, it is expected that turbulence decays with transient time t when there is no turbulent energy production. When mean velocity gradients are zero, the solutions of Eqs. (55) and (56) can be obtained analytically by using the modeling constant of C_2 (= 1.92) under the standard k-ε model. They are

$$k(t) = k_o\left(\frac{t_o}{t}\right)^a \tag{57}$$

$$\varepsilon(t) = \varepsilon_o\left(\frac{t_o}{t}\right)^{(a+1)} = \varepsilon_o\left(\frac{t_o}{k_o}\right)\left(\frac{k(t)}{t}\right) \tag{58}$$

where the exponent ***a*** in the equations is $1/(C_2 - 1)$ (≈ 1.09). During the energy cascade process with zero mean velocity gradients, k and ε values at the reference time, $t = t_o$, are k_o and ε_o, respectively. Turbulence kinetic energy will decay with about 1.1 exponent value in Eq. (57). It is demonstrated that the two-equation model predicts the power-law decay characteristics as observed in the Kolmogorov decay law.

5.0 EXAMPLE: VALIDATION OF THEORETICAL CONCEPT

As the previous review has shown, turbulent flows contain irregular motions over a wide range of length and time scales. The energy spectrum characterizes the turbulent kinetic energy distribution as a function of length scale, indicating the amount of turbulent kinetic energy contained in a specific length scale. Throughout the energy cascade, the turbulent eddy viscosity ν_t is a primary measure of length scale for momentum dissipation, and it is responsible for most of the mixing (Tennekes & Lumley 1972). When a chemical tracer or solid component introduced into the fluid is assumed to be mixed by the process of the turbulent energy cascade, key turbulence parameters such as turbulent dissipation rate and eddy viscosity are expected to provide a good signature or indicator of mixing performance.

The current work will primarily compare the Grenville-Tilton (G-T) correlation (Grenville & Tilton 1996) of the jet mixing time with CFD modeling results for their experimental tanks in an attempt to achieve a fundamental understanding of the turbulent jet mixing and to establish the usefulness and application of mixing indicators. These results will be also used to validate the principle of using key turbulence parameters as mixing indicators under three different conditions in a qualitative way. The three modeling conditions considered here are summarized in Table 4. These conditions are provided by Grenville & Tilton (1996).

Special care has been taken to explore the representation of the energy dissipation rate and turbulent eddy viscosity as these parameters are the drivers for turbulent mixing. The realizable k-ε model (RKE) in FLUENT has the option to use a new formulation for eddy viscosity, which includes the effect of vorticity transport. The current work is mainly based on the RKE model since the standard k- ε model is well known to be valid only for very large Reynolds number (i.e., greater than 10^6 Reynolds number). The RKE model uses new improved formulations for eddy viscosity and energy dissipation rate to include the dissipation effect of vorticity transport.

Table 4. Modeling conditions and G-T mixing times for transient CFD calculations

Tank	D (Tank dia.)	h_l (liquid height)	Inclination angle of Jet*	d_o (jet dia.)	U_o m/sec	Re_{jet}	Mixing time by G-T correlation
Tank A	1.68 m	1.55 m	42.6°	9.4 mm	2.2	20,680	758 sec.
Tank B	1.68 m	1.55 m	42.6°	26.1 mm	19.8	516,780	30 sec.
Tank C	36 m	11.16	17°	50 mm	19.5	975,000	4371 sec.

Note: *Jet is located at the corner of tank bottom as shown in Fig. 6.

5.1 Mesh Sensitivity Study

Basic strategy of the CFD method is to replace the continuous problem domain with a discrete domain using a grid. In this work, grid sensitivity analyses were performed to make sure that the numerical solutions are insensitive to the grid sizes of the entire computational

domain. Three different mesh sizes were applied to assess their impact on the flow solutions for two configurations of Tank B and Tank C as shown in Table 5. The grid was refined based on gradients in the velocity magnitude, with the location of the adapted cells being concentrated around the jet mainstream. The steady flow solutions coupled with the RKE turbulence model were used to determine the regions of highest velocity gradients for the gradient-based adaptation. Each tank was refined two times and the overall mesh size was increased approximately 30% during each grid refinement. The second grid refinement was based on regions of highest velocity gradients in the previously adapted regions in order to provide further mesh density in the regions surrounding the jet mainstream. Table 4 provides the number of nodes used in each of the grid refinements.

Simulations were performed on two different computational platforms: SUN Enterprise 6900 server with 48 CPUs (1.5 GHz) and 388 GB of RAM; and SUN Ultra 40 workstation with 4 CPUs (2.4 GHz) and 16 GB of RAM. To measure the computational performance across all configurations, the total clock time for each simulation (20,600 iterations) is normalized per 1 million finite volumes and 4 CPUs. Given these stipulations, simulations using RKE required approximately 50 hrs of clock time on the workstation and 80 hrs on the server.

Appropriate combinations of time step size and iterations per time step were determined by an optimization study. For the baseline Tank B, a time step size of 0.004 s was used for $0 < t < 4$ s (1000 time steps), a time step size of 0.04 s was used for $4 < t < 8$ s (100 time steps), and a time step size of 0.2 s was used for $8 < t < 200$ s (960 time steps). The expected mixing time for this configuration was on the order of 30 s. These numbers were scaled for Tanks A and C based on the relative expected mixing time. For Tank A, the incremental time steps sizes were 0.1, 1, and 5 s. For Tank C, the incremental time steps sizes were 0.6, 6, and 30 s. Note that the total number of time steps (2060) and the iterations per time step (10) were kept constant for all simulations. Thus each simulation required 20,600 iterations to go from $t = 0$ to a flow time equivalent to 5 times the expected mixing time from Grenville and Tilton (1996, 1997).

During the numerical simulation of jet flow in each of the three tanks, nine locations inside the tank were monitored as shown in Fig. 7. The time history of the nondimensionalized velocity magnitudes at point 4 and point 8 for the baseline and two refinement cases of Tank B is shown in Fig. 8. Transient times in Fig. 8 are nondimensionalized with respect to the time estimated by Grenville-Tilton correlation. As can be seen in figure, the point 4 mixing time for the refinement 1, Adapt_1 mesh, was about 48 seconds while the mixing time for refinement 2, Adapt_2 mesh, was about 51 seconds. The mixing time predicted with the baseline mesh produces an error of less than 10 % as compared to the Adapt_2 mesh. The impacts of the mesh refinements on the turbulent kinetic energy and turbulent viscosity for the Tank B configuration are presented in Figs. 9 and 10. As can be seen in the figures, the turbulent kinetic energy for the refined cases takes longer to settle into its quasi-steady values and exhibits low frequency oscillations about the average equilibrium value for flow times greater than 200 seconds. The sensitivity results for Tank C geometry are also presented in Figs. 11 to 13. Thus, the baseline mesh gives a reasonable estimate of mixing time and the added computational expense of a more refined mesh does not significantly improve the results. The adaptation meshing does result in different initial transient behavior. However, the main concern in determining an appropriate mesh resolution is the effect on the predicted mixing time and the differences in the initial transient behavior are not of primary concern. The primary objective of these studies is to validate the theoretical concept that the eddy viscosity and turbulent dissipation rate can be used as potential measures of mixing performance in a tank.

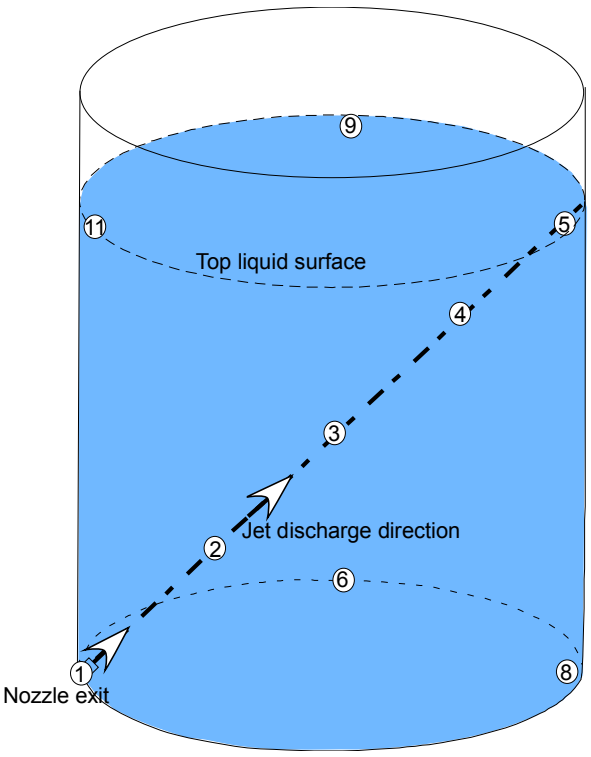

Figure 7. Locations of nine monitoring points in the flow field domain driven by jet mixer inside the tank

Table 5. Number of mesh nodes used in grid sensitivity study for Tank B and Tank C

Tank configuration	Baseline mesh (Original)	Refinement 1 (Adapt_1)	Refinement 2 (Adapt_2)
Tank B	296,000	381,000	504,000
Tank C	275,000	354,000	462,000

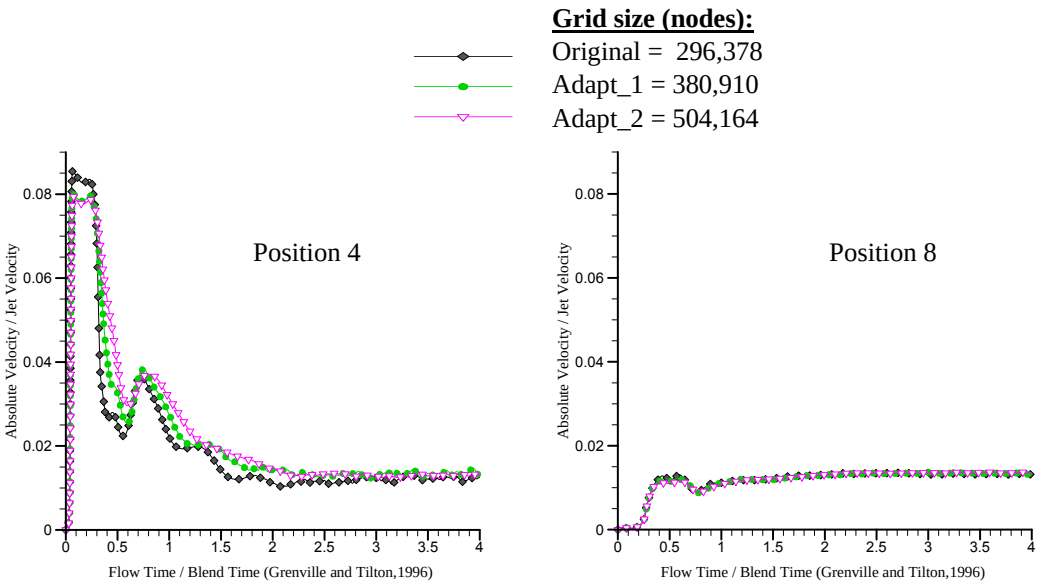

Figure 8. Mesh sensitivity results for transient nondimensionalized velocity magnitudes at two monitoring locations point 4 and point 8 inside Tank B

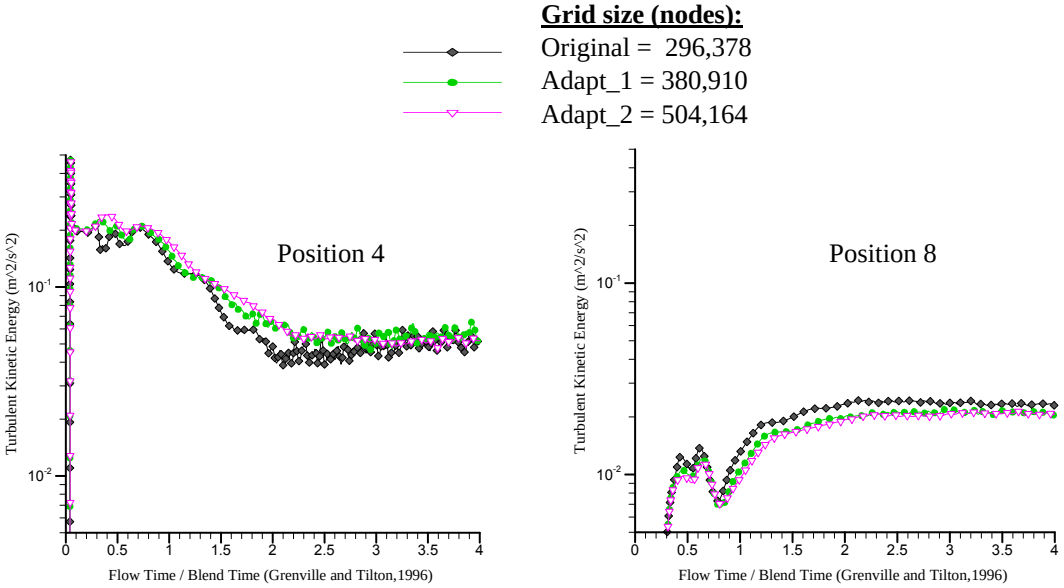

Figure 9. Mesh sensitivity results for transient kinetic energies at two monitoring locations point 4 and point 8 inside Tank B

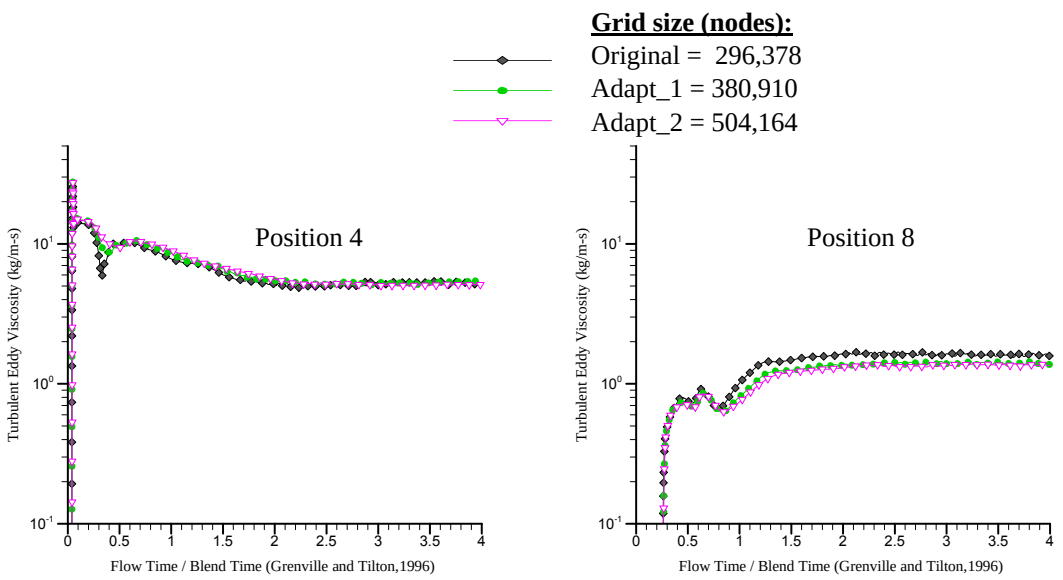

Figure 10. Mesh sensitivity results for transient eddy viscosities at two monitoring locations point 4 and point 8 inside Tank B

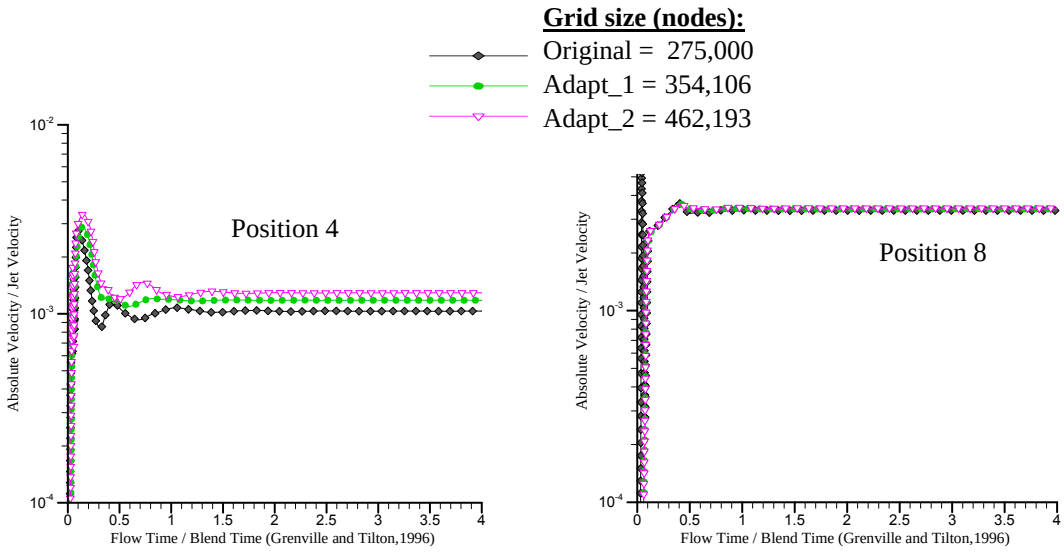

Figure 11. Mesh sensitivity results for transient nondimensionalized velocity magnitudes at two monitoring locations point 4 and point 8 inside Tank C

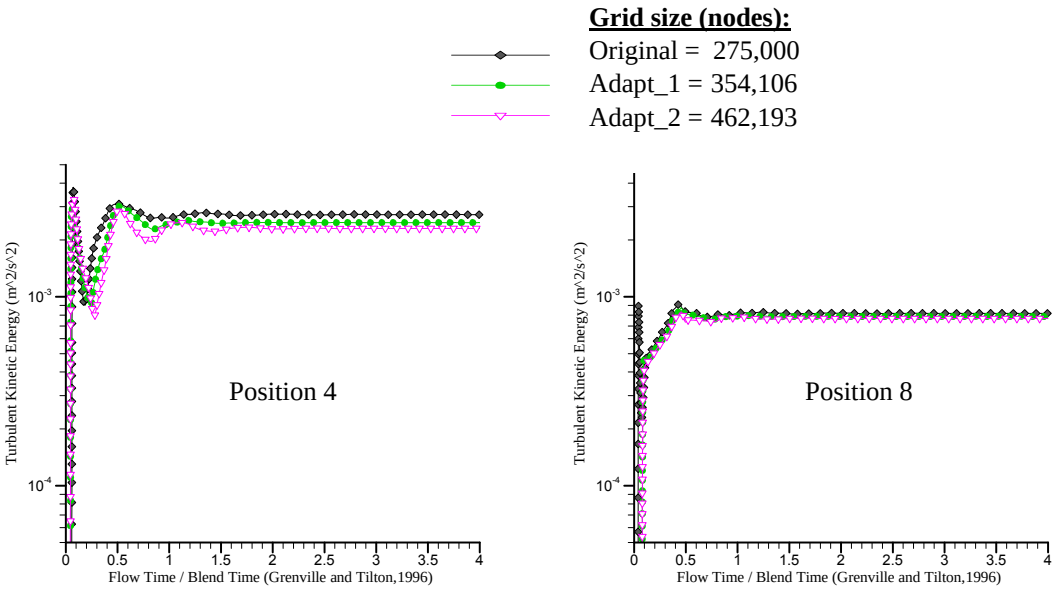

Figure 12. Mesh sensitivity results for transient kinetic energies at two monitoring locations point 4 and point 8 inside Tank C

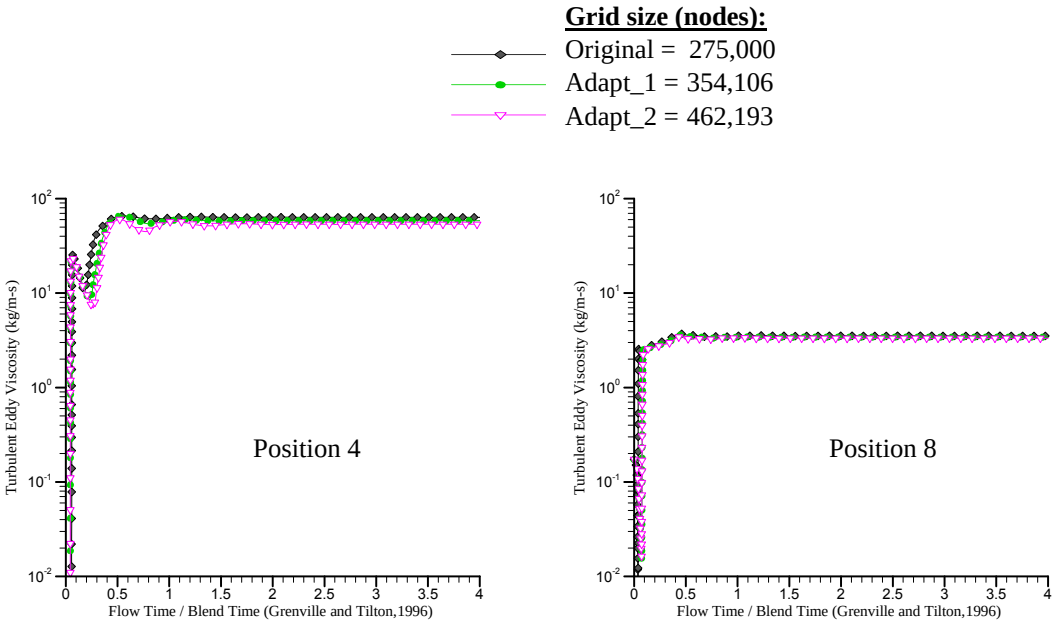

Figure 13. Mesh sensitivity results for transient turbulent viscosities at two monitoring locations point 4 and point 8 inside Tank C

5.2 CFD Results against Grenville-Tilton Correlation for Mixing Time

The prediction of the transient response of submersible jet flows in a quiescent fluid medium is based here on the incompressible continuity and Navier-Stokes (N-S) equation with the RKE turbulence model. Figure 14 shows the transient flow evolution along the principal direction of jet discharge in Tank B. It is noted that local jet velocities along the jet axis decay rapidly by about 80% of initial jet velocity at a distance of 20 times jet diameter from the jet exit due to the local momentum dissipation into the stagnant liquid. The dissipated momentum induces fluid mixing via liquid entrainment into the jet flow region as illustrated in Fig. 4. Figure 15 shows transient snapshots for the flow evolution in the symmetry plane driven by the jet with a 26.1-mm diameter located at the bottom of Tank B. Transient snapshots of flow evolution in horizontal planes at two different tank elevations, 0.2 m and 1.2 m above the jet, are presented in Fig. 16. The results show a transient maximum local velocity at the 1.2 m elevation occurring in about 30 seconds. While these results show the qualitative development of the jet profile, the quantitative results are questionable and emphasize the need to evaluate the impact of boundary conditions on the flow solution. In this case, the use of a fixed wall boundary to represent the top fluid boundary may be causing unrealistic behavior in the jet development over time. This will be investigated as part of the continuing work.

Transient local velocity magnitudes at two monitoring locations on the principal discharge direction, points 4 and 5, inside Tank B are shown in Fig. 17. The results show that it takes about 45 seconds for local jet velocity at point 4 (about 1.7 m from the jet nozzle) to reach quasi-steady state. The corresponding kinetic energies and energy dissipation rates are presented in Figs. 18 and 19. As discussed previously, eddy viscosity ν_t is the proportionality constant within the derivative of the Reynolds stress in the N-S equation to describe the rate of energy dissipation. Transient turbulent viscosities at these two monitoring locations on the principal discharge direction inside Tank B are shown in Fig. 20.

The spreading of the jetted fluid is retarded by the interaction with the tank floor and top free surface as shown in Fig. 3, and the inner part of the flow may be expected to show a certain structural similarity to a boundary layer. Entrainment of quiescent fluid occurs near the outer edges of the flow. In this case, sludge solids settled near the edge of the boundary region are entrained into a turbulent zone, and they are suspended and mixed. Figure 21 shows transient local velocity magnitudes at two monitoring locations near the tank floor (point 8) and top free surface (point 9) inside Tank B. The transient results show that a quasi-steady velocity of about 0.3 m/sec is maintained near the tank floor in about 40 seconds after initiation of the jet, resulting in turbulent kinetic energy per unit mass (k) of 0.02 m^2/sec^2. The transient turbulent energies at the two remote monitoring points approach a quasi-steady value of ~0.02 m^2/sec^2 as shown in Fig. 22. When quasi-steady state is reached, this kinetic energy fed to the fluid medium will be dissipated at a rate of 0.02 m^2/sec^3 as shown in Fig. 23. In this case quasi-steady turbulent viscosity is about 1.5 kg/m-sec as shown in Fig. 24. It is noted that the turbulent viscosity is about 1,500 times higher than molecular viscosity since Reynolds number is in the range of 500,000.

Figure 25 compares transient velocity magnitudes at a monitoring point 4, Fig. 6, on the main stream direction of jet discharge for a wide range of Reynolds numbers, 2×10^4 to 10^6. As shown in the figure, a quasi-steady condition is reached at the mixing time predicted by the G-T correlation. Comparisons of the transient turbulence behaviors for kinetic energy and turbulent viscosity are made for the same range of Reynolds number as presented in

Figs. 26 and 27. The corresponding results for the remote region, point 8, are shown in Figs. 28 to 30.

As shown in the example results, transient behaviors of k and ε are consistent with turbulent eddy viscosity ν_t. The eddy viscosities were calculated from the RKE turbulence model involving turbulent kinetic energy (k) and its dissipation rate (ε) coupled with time- and space-averaged N-S equations. The CFD modeling results demonstrate that the time evolution of the turbulent eddy viscosity bears a reasonable similarity to the mixing time based on the G-T correlation.

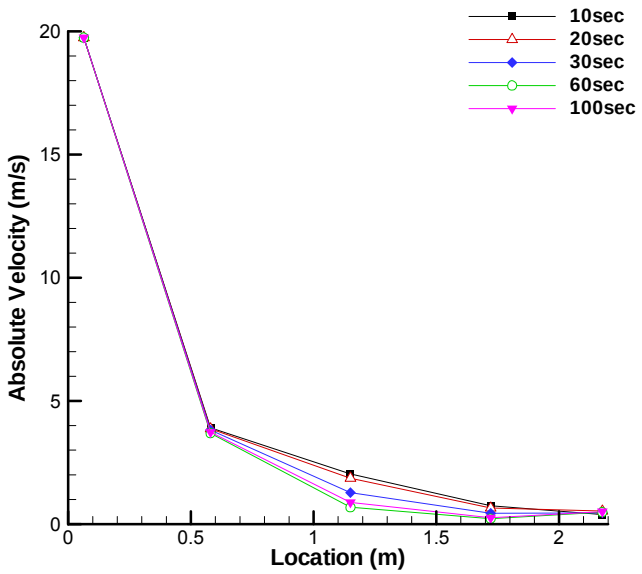

Figure 14. Transient turbulent flow evolutions along the principal direction of jet discharge in tank B

5.3 Initial Conditions

The significance of convection and turbulent dispersion is addressed in some detail by Patwardhan et al. (2003) through an evaluation of several types of mixers, one of which is a turbulent jet. They characterize the effectiveness of the mixers in terms of the partitioning of the input energy between bulk convective flow and the turbulent dispersion process. In their work, they observe that the slower of these two blending processes is the convective term, and that the turbulent dispersion process is fast compared to the bulk convection.

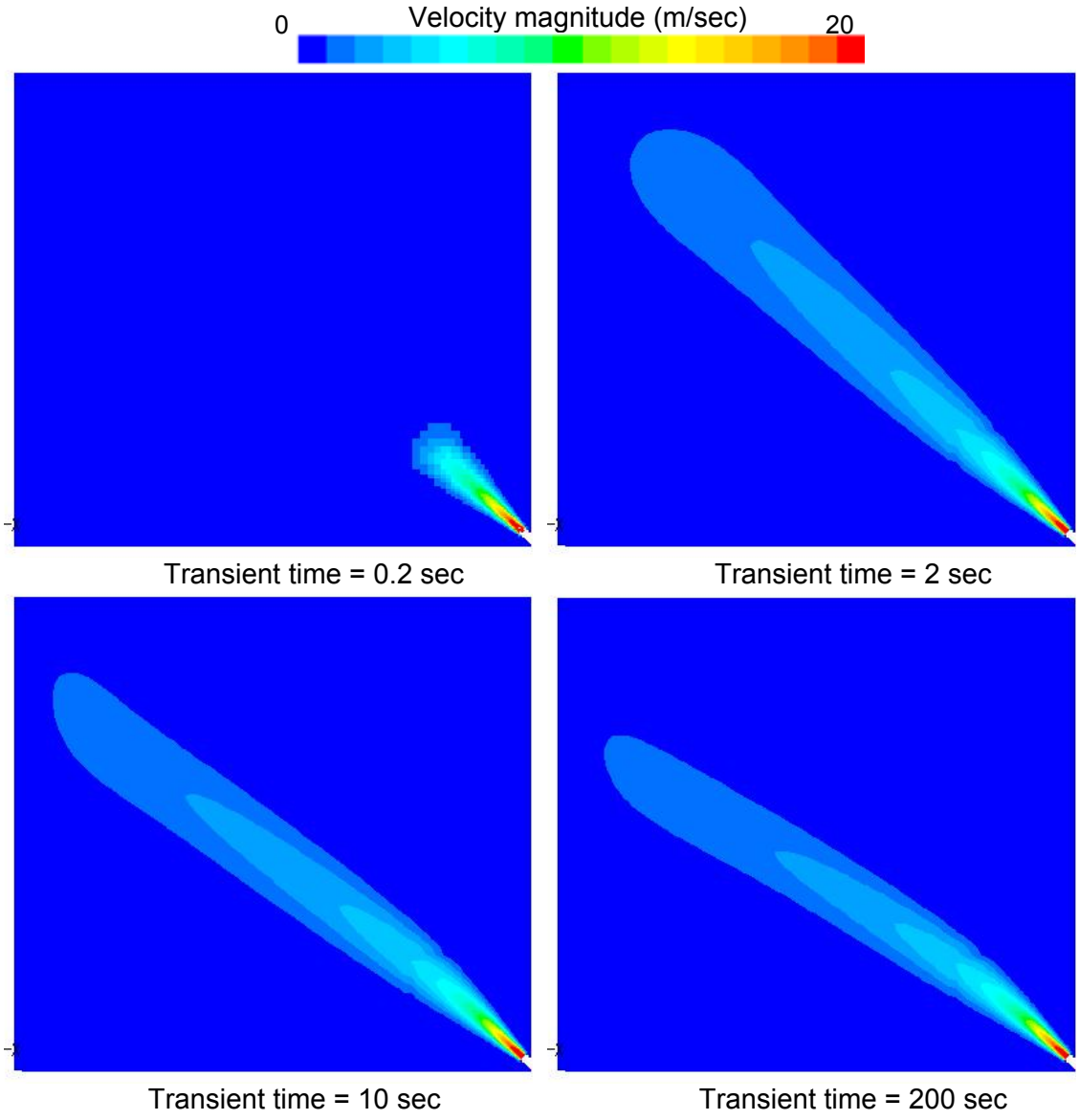

Figure 15. Transient flow evolutions at the plane of jet discharge in tank B using RKE turbulence model

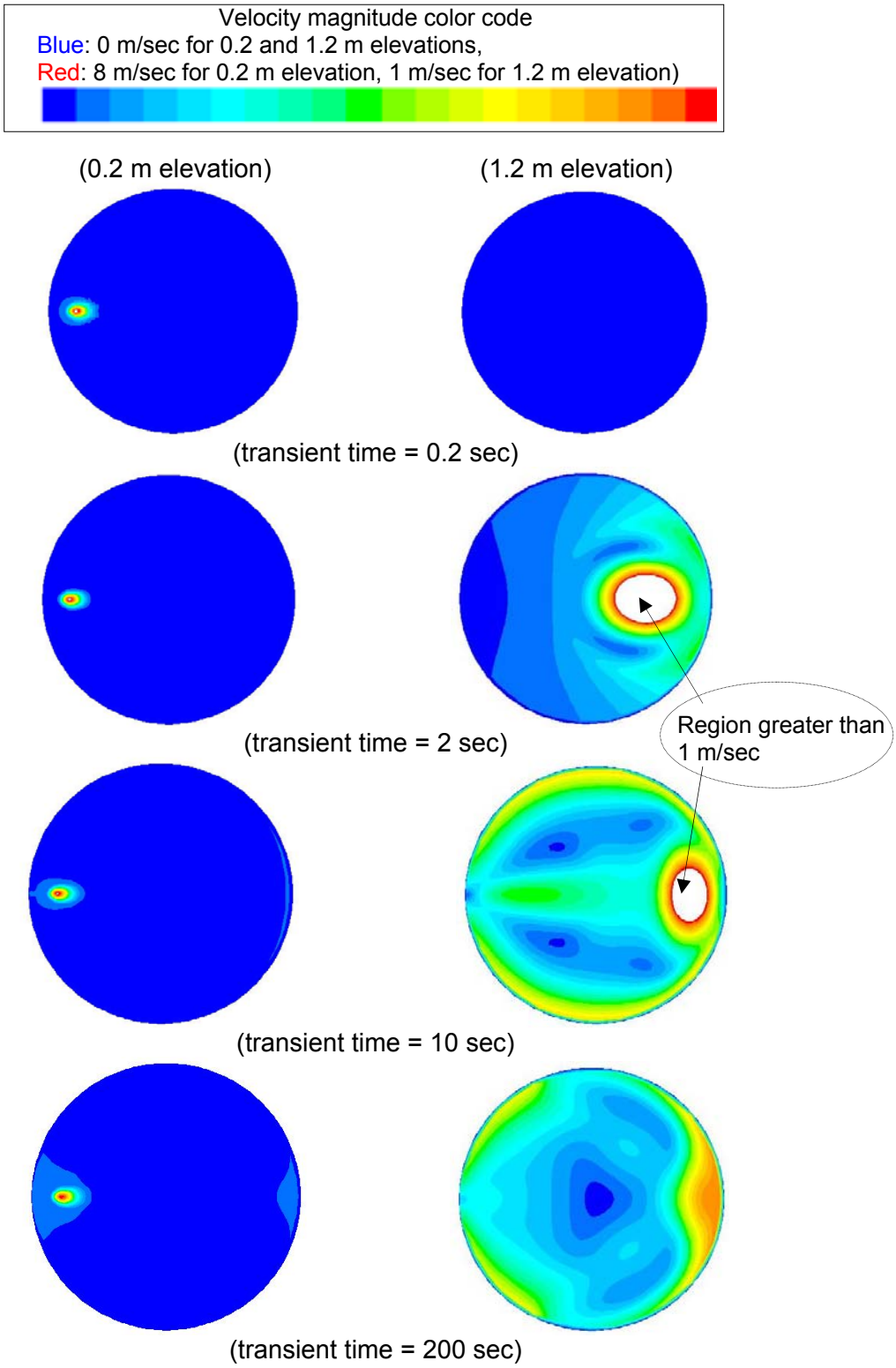

Figure 16. Transient snapshots of flow evolutions at the horizontal planes at two different tank elevations of 0.2 m and 1.2 m in tank B using RKE turbulence model

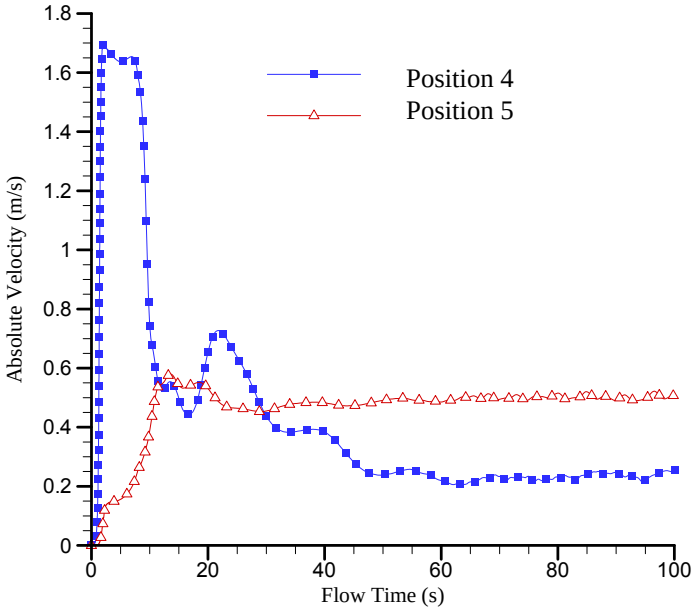

Figure 17. Transient local velocity magnitudes at two monitoring locations on the principal discharge direction inside Tank B

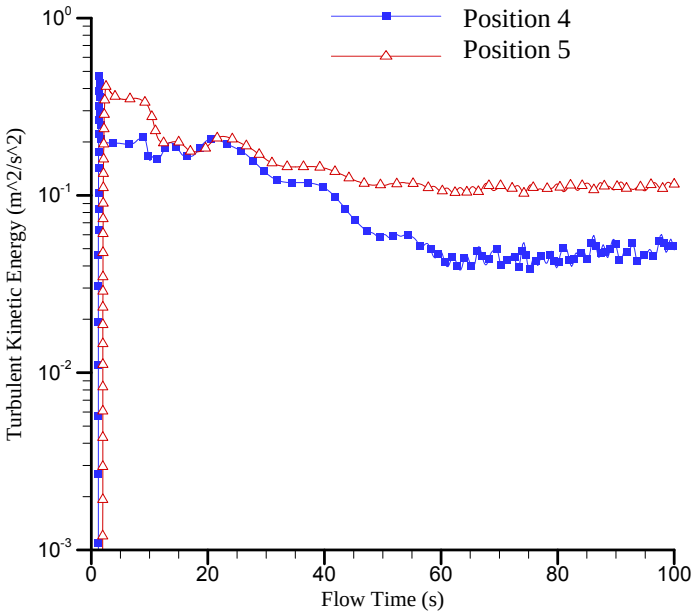

Figure 18. Transient turbulent kinetic energies at two monitoring locations on the principal discharge direction inside Tank B

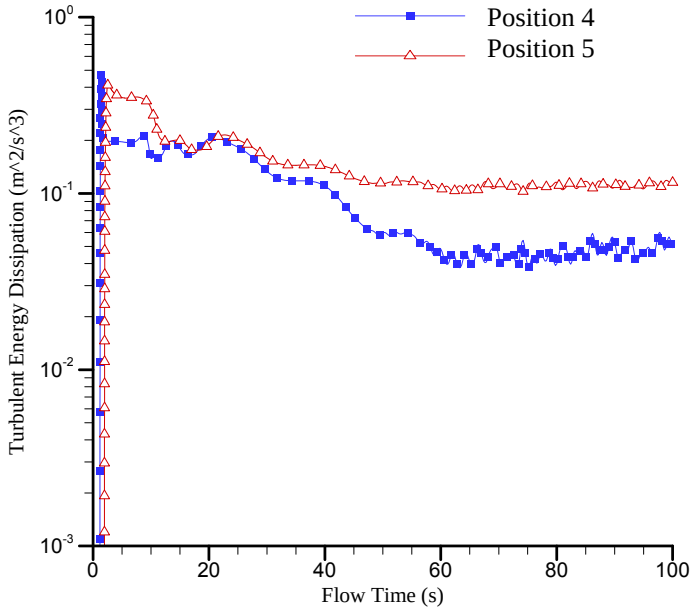

Figure 19. Transient turbulent energy dissipation rates at two monitoring locations on the principal discharge direction inside Tank B

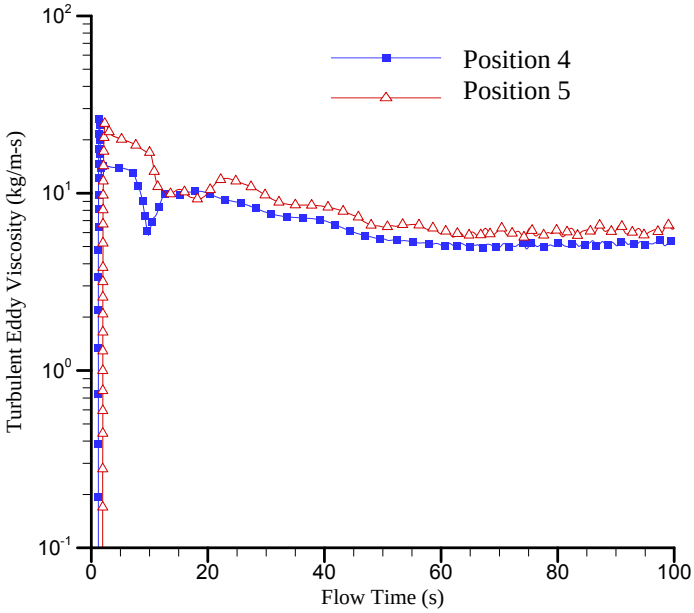

Figure 20. Transient turbulent viscosities at two monitoring locations on the principal discharge direction inside Tank B

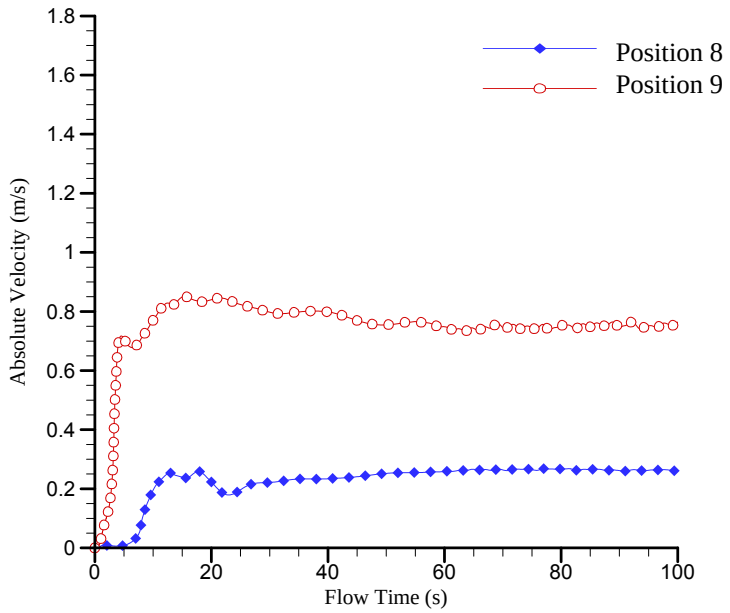

Figure 21. Transient local velocity magnitudes at two monitoring locations far away from the principal discharge line inside Tank B

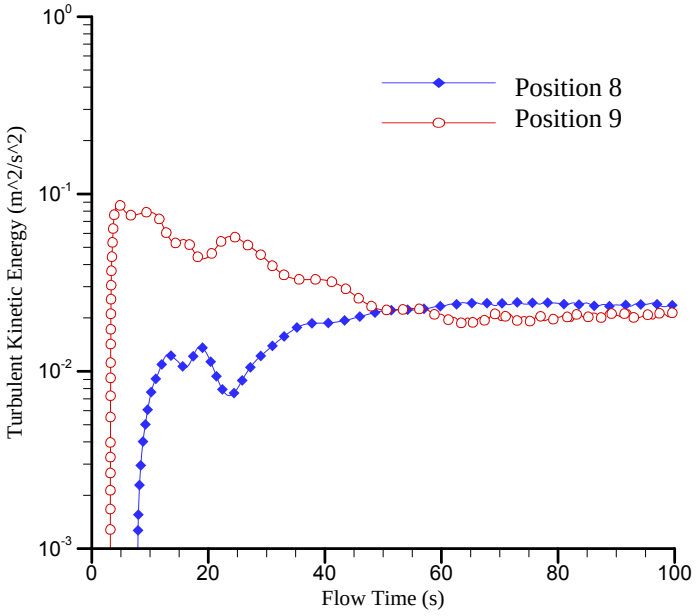

Figure 22. Transient turbulent kinetic energies at two monitoring locations far away from the principal discharge line inside Tank B

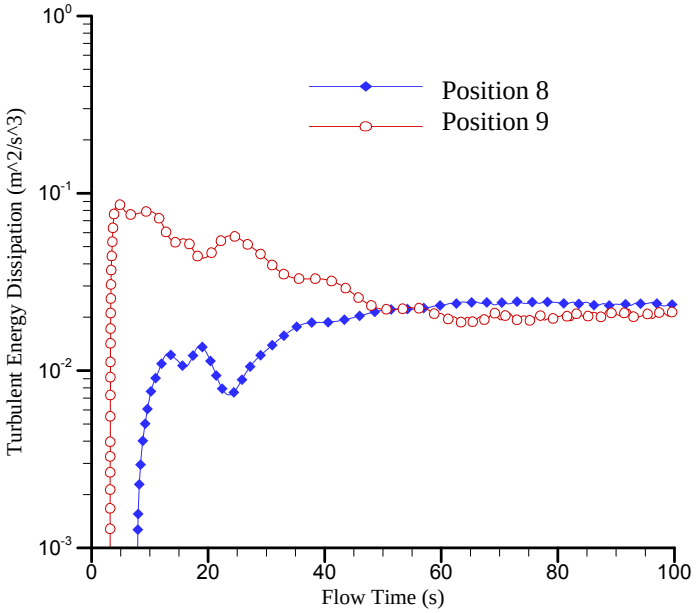

Figure 23. Transient turbulent energy dissipation rates at two monitoring locations far away from the principal discharge line inside Tank B

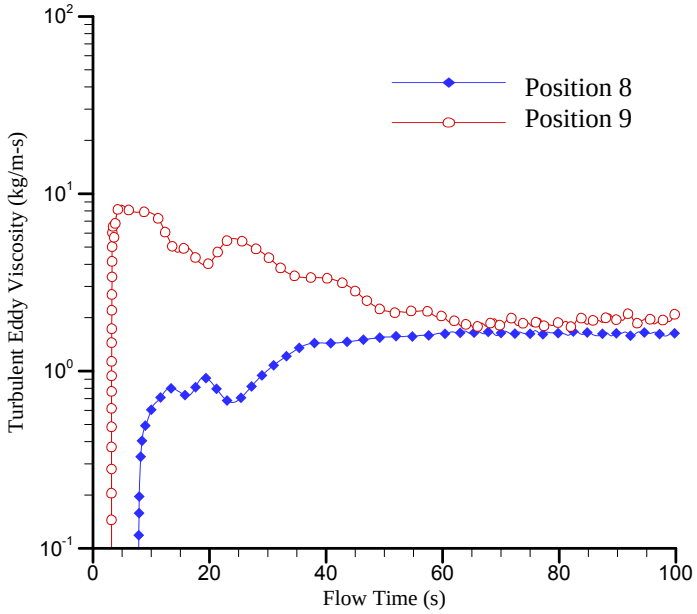

Figure 24. Transient turbulent eddy viscosities at two monitoring locations far away from the principal discharge line inside Tank B

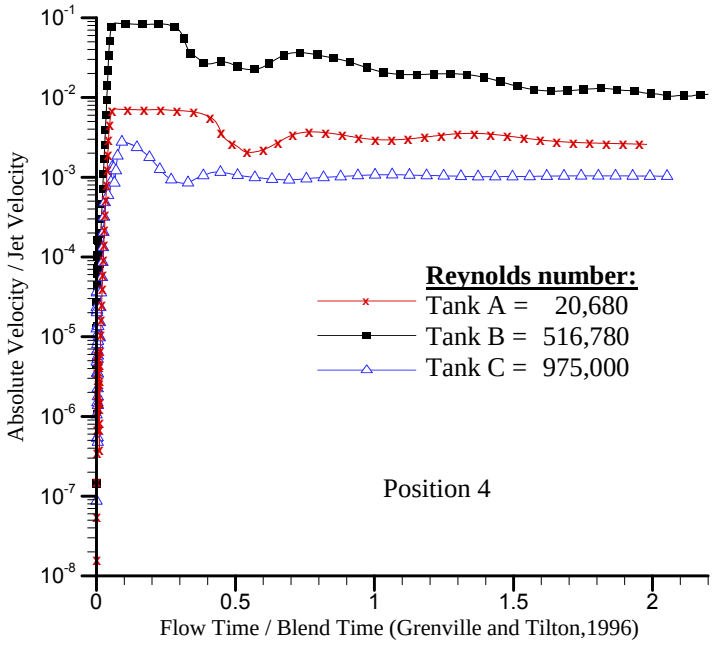

Figure 25. Comparison of transient velocity magnitudes at a monitoring location 4 on the principal discharge line for three different operating conditions (RKE turbulence model)

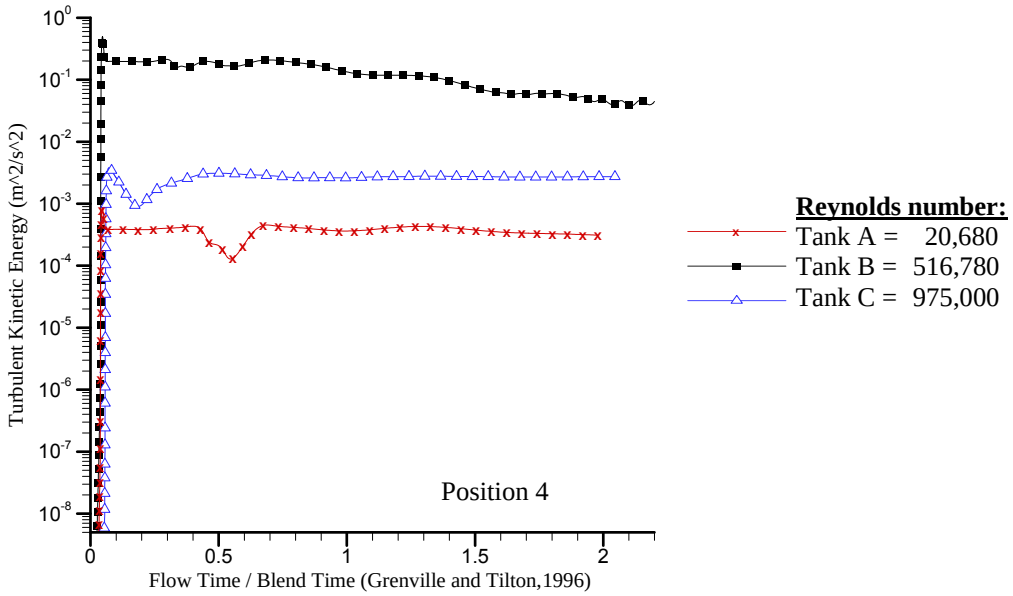

Figure 26. Comparison of transient turbulent kinetic energies at a monitoring location 4 on the principal discharge line for three different operating conditions (RKE turbulence model)

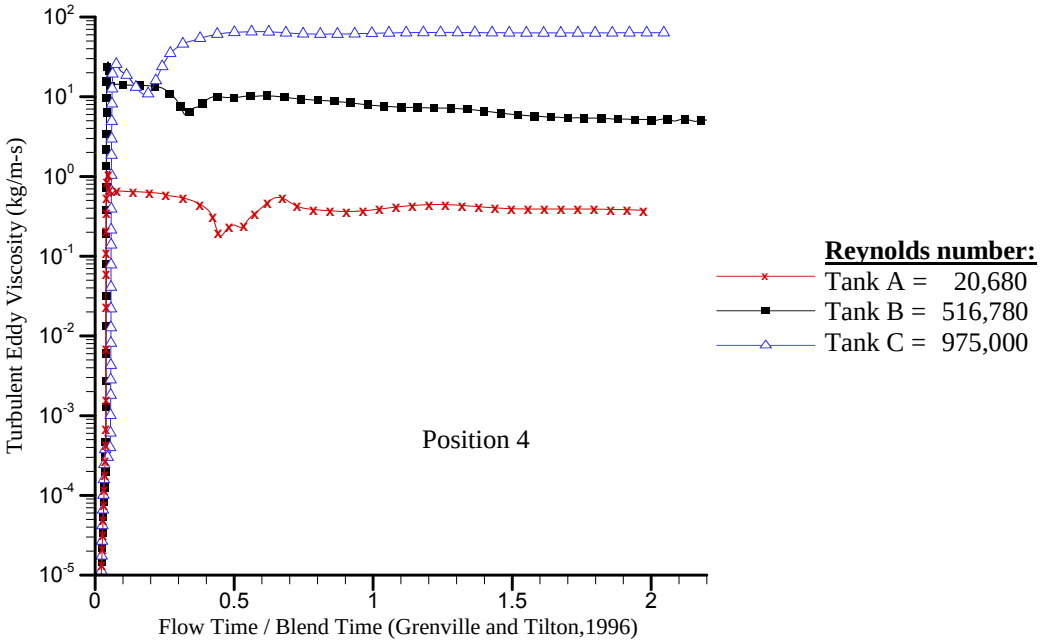

Figure 27. Comparison of transient turbulent eddy viscosities at a monitoring location 4 on the principal discharge line for three different operating conditions (RKE turbulence model)

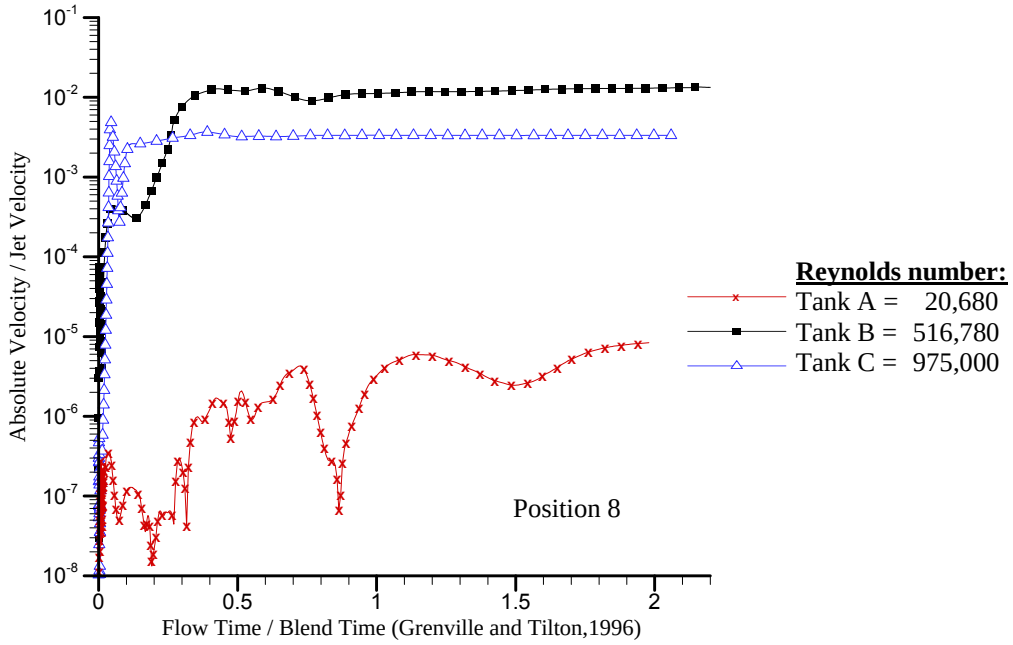

Figure 28. Comparison of transient velocity magnitudes at a monitoring location 8 far away from the principal discharge line for three different operating conditions (RKE turbulence model)

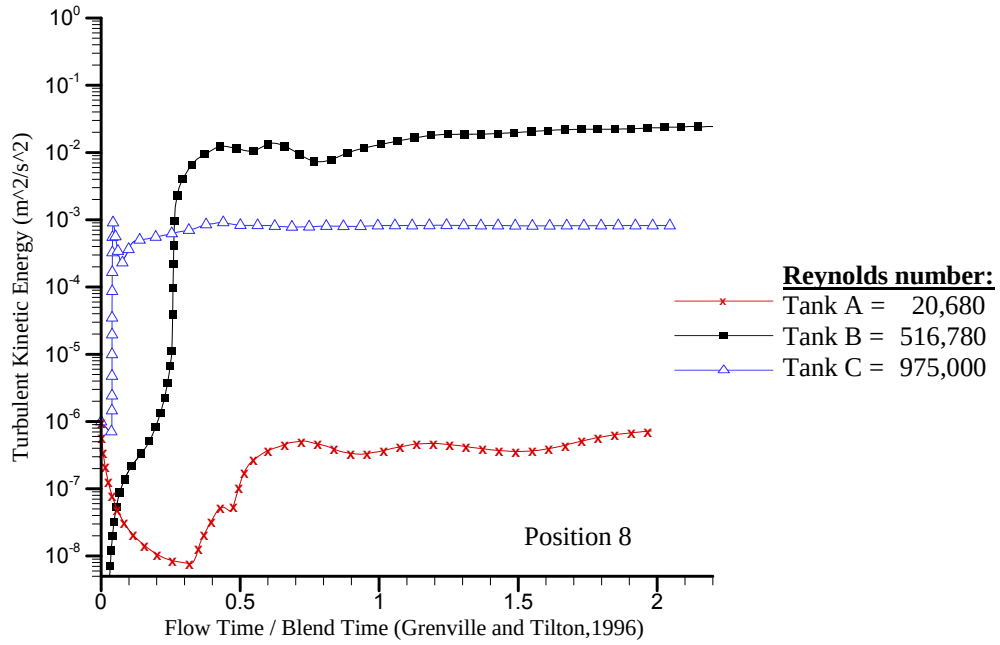

Figure 29. Comparison of transient turbulent kinetic energies at a monitoring location 8 far away from the principal discharge line for three different operating conditions (RKE turbulence model)

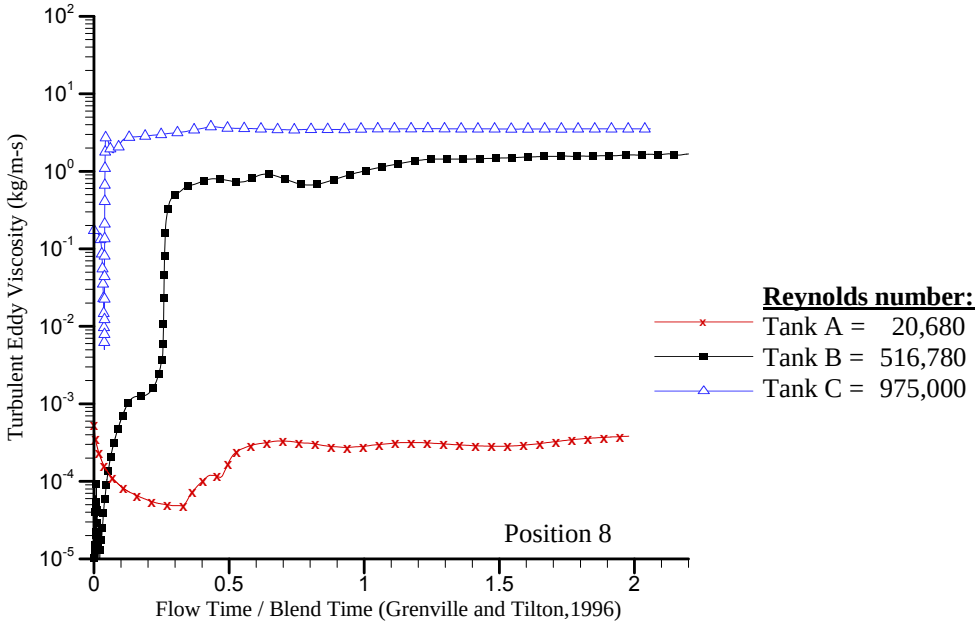

Figure 30. Comparison of transient turbulent eddy viscosities at a monitoring location 8 far away from the principal discharge line for three different operating conditions (RKE turbulence model)

With this in mind, it is helpful to identify a marker that may be used to measure the time required for a scalar to be propagated throughout the vessel being mixed, and thereby measure the time required for mixing to occur throughout the vessel. One such measure is the Taylor Reynolds number, Re_T. A value of $Re_T = 100$ has been suggested as an indication of a sufficient level of turbulence to provide local mixing (Dimotakis 2000), i.e., the dissipation of local gradients in scalar quantities. If it can be established that this threshold value has been developed throughout the vessel, then one can conclude that sufficient turbulence has been demonstrated to ensure mixing of the vessel contents. This observation would be expected to hold in a transient sense as well as when the fluids being mixed are miscible, and therefore unlikely to separate even if the level of turbulence decreases with time.

Re_T can also be used as a marker for convective transport through the eddy regions, and especially the large eddies that are already present in a fully developed flow, if the bulk flow pattern in the vessel is established quickly compared to that convective transport time. This behavior has been observed in the calculations for this report, as well as in earlier work (Lee et al. 2004, 2008) focused on rotating jet pumps in a Savannah River waste tank. This convective behavior remains the limiting phenomenon for establishing a mixed condition, and it is essentially independent of the tank initial conditions. Because the bulk flow patterns are established quickly – especially for an incompressible flow (Lee et al. 2004, 2008) – the transient evolution time measured for the startup can be shown to be an appropriate estimate of the mixing time even for the injection of a scalar into a fully developed flow in a vessel.

The fact that a turbulence marker such as Re_T could be used to measure the time required to establish a mixed condition in the tank is obvious if the mixing transient starts from a quiescent condition. The fact that this same mixing time applies to the injection of a scalar concentration into a tank with a fully developed flow profile is not so obvious. The starting condition in the tank is obviously different, but it is not likely that this difference affects the mixing time significantly. The energy needed to distribute turbulence kinetic energy throughout the tank consists of two parts, the kinetic energy of the bulk flow and the turbulence kinetic energy that propagates through the eddies and dissipates the scalar gradients. The former is the far greater term, and it serves to establish the overall flow pattern in the tank. The pattern develops quickly when the jet is first introduced into the stagnant tank, largely because the flow is incompressible (or nearly so), so pressure propagates throughout the tank essentially instantaneously. The only transient that must occur to establish the flow pattern is that of performing the work necessary to establish the bulk kinetic energy of the mean flow. The power supplied by the incoming jet is sufficient to accomplish this quickly. The far longer contributor to the mixing time is the propagation of the scalar (or the turbulence marker) through the eddy regions, and this transient is the same whether the mixing started from fully developed or from stagnant conditions.

This realization led to a second set of calculations designed to test the mixing behavior for a scalar concentration injected into a fully developed tank, and to compare the results to those obtained for stagnant initial conditions. At the same time, this second set of calculations tested the concept of using the propagation of Re_T as a measure of mixing.

A new model of the Tank B configuration was set up with the return path reflecting the actual tank configuration as described by Grenville (2009). The new model configuration is shown in Fig. 31. As show in the figure, a jet pump with 42.6^o upward angle is located at the tank bottom, and the jetted flow returns to the pump through the tank bottom. Based the new

model, the calculations for two separate cases were performed. The first case is the transient flow evolution calculations of submersible jet flows in a quiescent fluid medium as performed for the earlier analysis. The second case is another transient modeling approach based on another set of species balance equation in addition to the continuity, momentum, and two turbulence equations. In this approach, the transient calculations were started from the fully developed flow distribution of the first case runs as initial conditions. The second approach simulates the mixing tests performed by Grenville and Tilton (1996). For the first case, a transient run was started from stagnant conditions and run until a fully developed, stable profile was established. The results are consistent with the earlier one as shown in Fig. 15. Figure 32 shows the fully developed flow patterns established by the first approach. The second was transient calculation for a contaminant species started from the fully developed condition of the first run in which the species was injected for 10 seconds into the inlet jet. In this case, the species fluid was an acid of 1.14 specific gravity and 1.16 cp viscosity, and total volume injected through 10 mm hole was about 0.21 gallons for the initial period of 10 seconds. Detailed test configurations of the Tank B system are shown in Fig. 31. The transient contaminant profile was then calculated and observed. The comparison of these two calculations is shown in Figure 33. The results show very clearly that the injected contaminant species follows the velocity profile and that the propagation of the contaminant species develops over the same time period as both the bulk flow and the eddy flow patterns.

A more detailed look at the Tank B concentrations is shown in Figure 34. The ratio of the local concentration to the equilibrium concentration shows good agreement between the steady state ratio at point 6 in the tank, the location identified as the last to mix. The agreement with the Grenville-Tilton results is very good.

Figure 35 shows a similar calculation for the three tank configurations used earlier in this report, but the results are determined using the Taylor Reynolds number. Again, the comparison with Grenville-Tilton is very good, even though these calculations were performed from a stagnant starting condition. The fact that the mixing time is the same is significant.

Figure 36 shows a similar comparison for mixing in a horizontal tank using a jet mixer (Perona et al. 1994). The results show that the Taylor Reynolds number is similar to that seen for the Grenville-Tilton tank calculations when a mixed condition is established, in this case Re_T in the range of 25 – 60.

Figure 37 shows the value of Re_T for the Grenville-Tilton data and the ORNL data together. It demonstrates that the relationship between the jet Reynolds number and the final Taylor Reynolds number for a mixed condition is smooth for the combined data set, a further indication that the initial conditions do not have a significant impact on the propagation of a scalar through the eddy regions of the tanks.

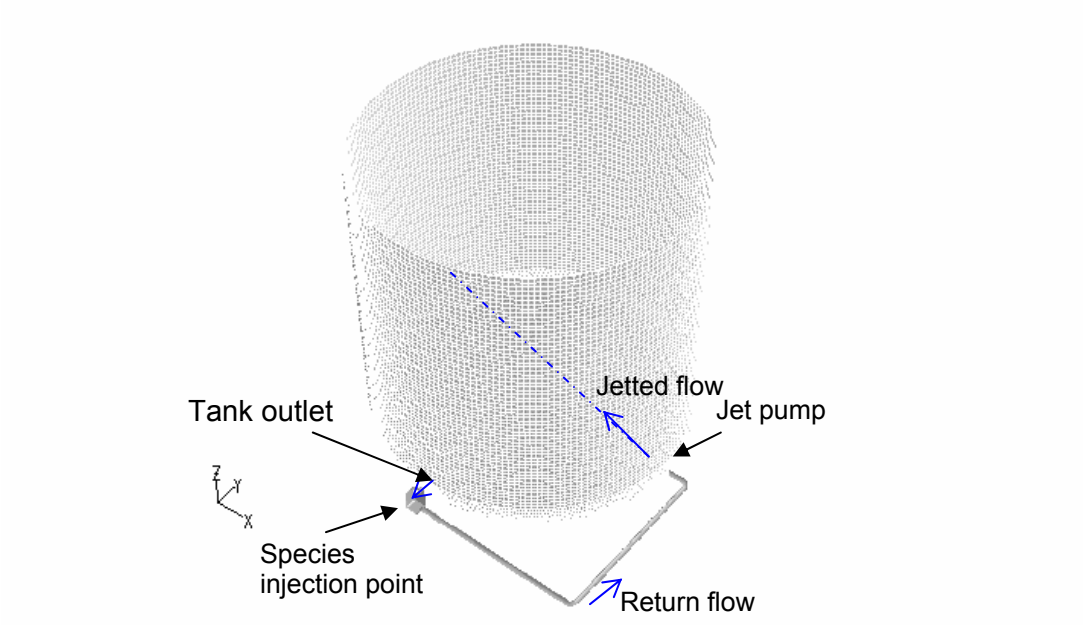

Figure 31 Tank B geometry for the demonstration runs based on two different approaches of transient flow pattern and species transport calculations

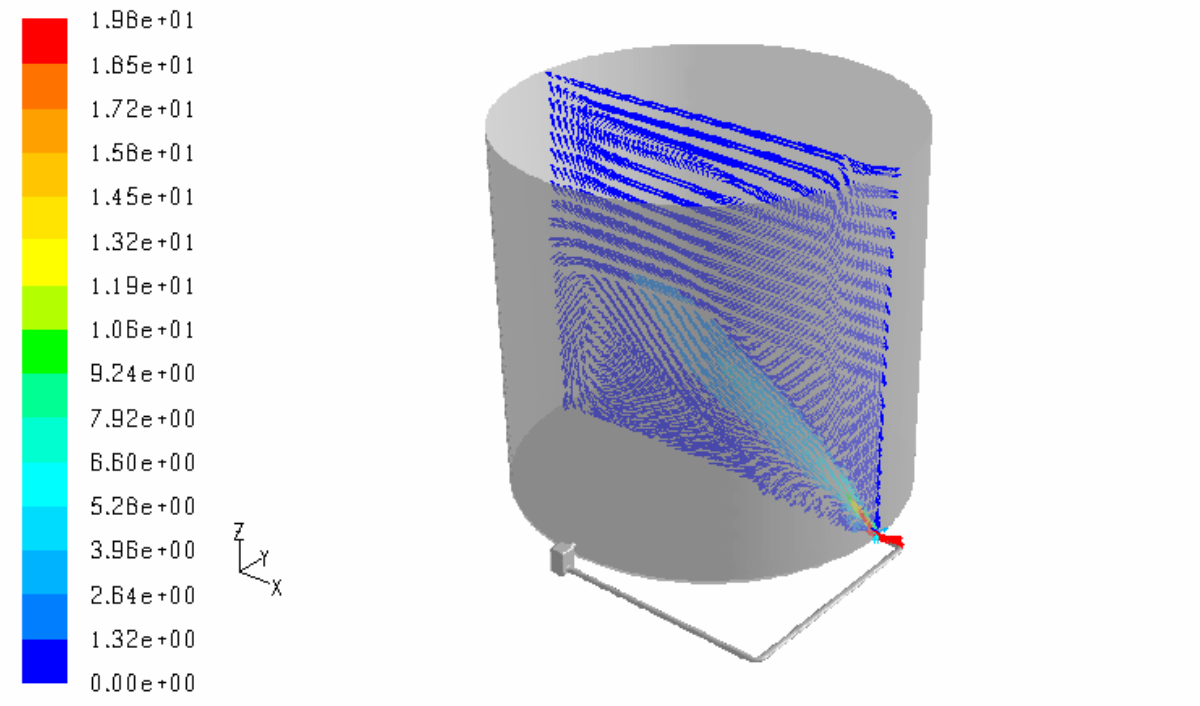

Figure 32. Fully developed flow patterns used for the transient calculations of contaminant species

(2^{nd} Case: Species conc.) (1^{st} Case: Velocity flow patterns)

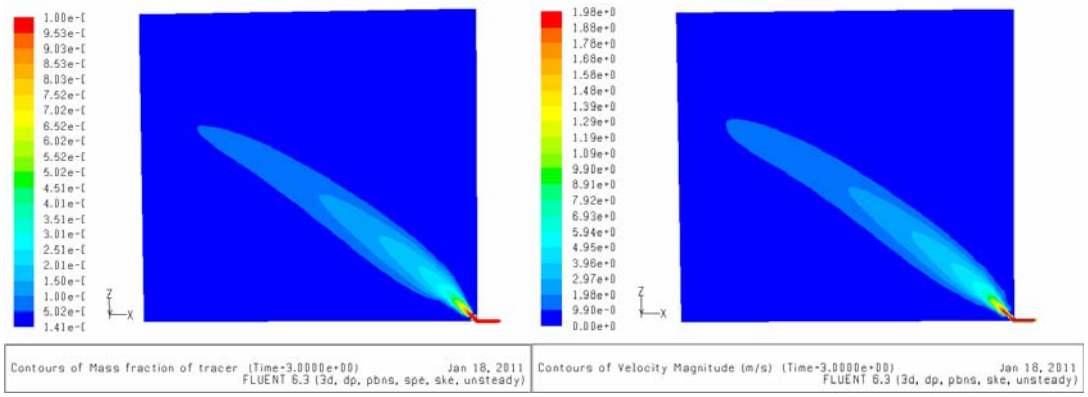

(t = 3 sec)

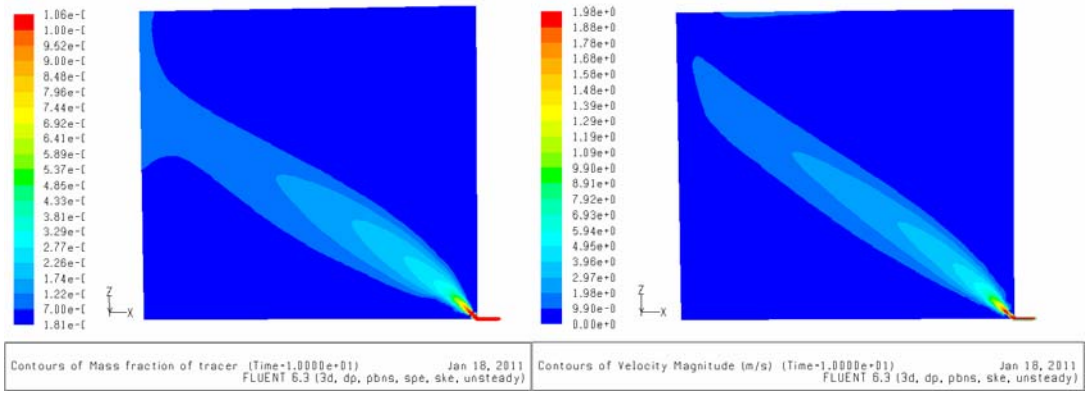

(t = 10 sec)

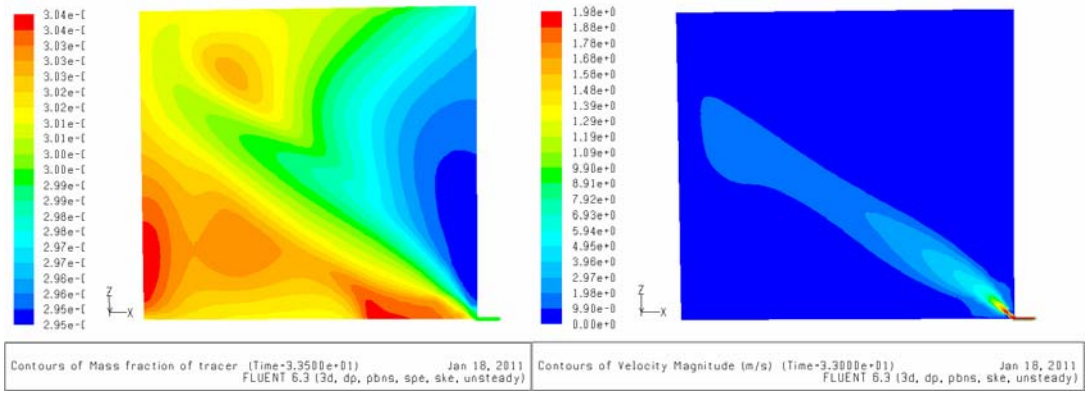

(t = 33 sec)

Figure 33. Comparison of transient snapshots between species concentration and flow patterns (Equil. species conc = 3.02×10^{-4})

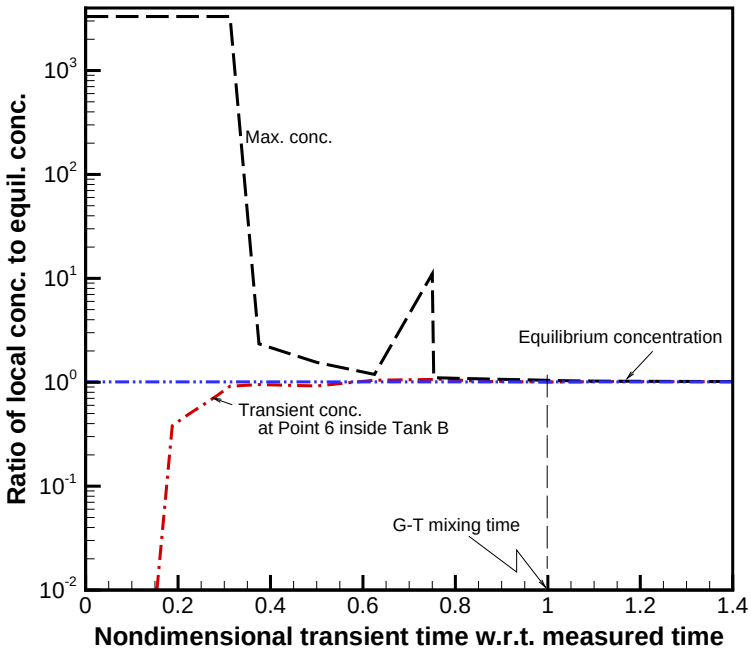

Figure 34. Transient species concentrations observed at point 6 in Tank B based on the mixing model coupled with species transport equations (G-T mixing time = 32 sec.)

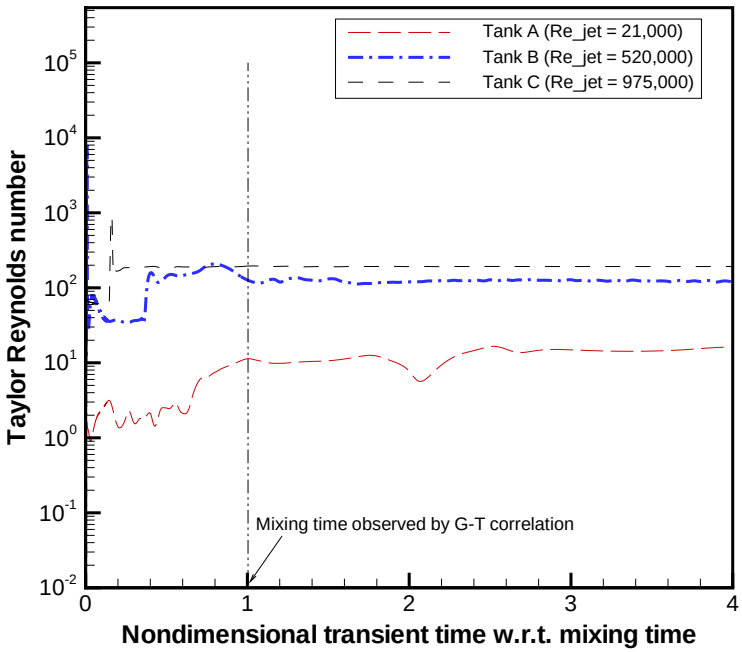

Figure 35. Taylor Reynolds number vs. mixing time

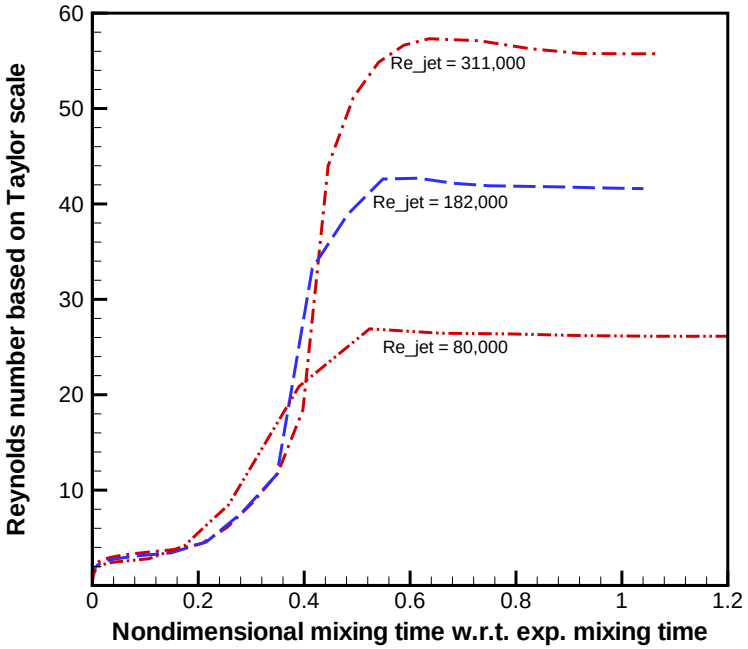

Figure 36. Transient Reynolds number based on Taylor lengthscales for horizontal jet in horizontal cylindrical tank with 10 ft diameter and 40 ft long (ORNL)

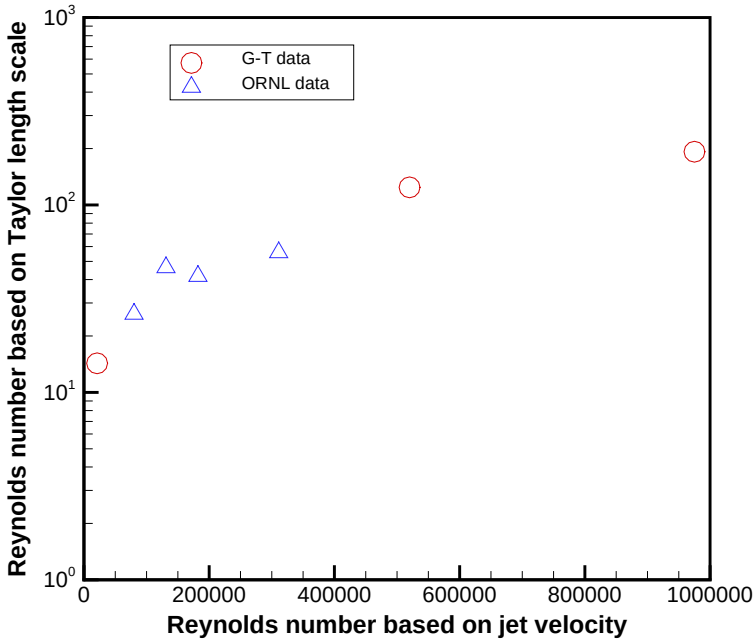

Figure 37. Taylor Reynolds number for various jet Reynolds numbers at the slowest locations

6.0 ANALYSIS AND EVALUATIONS

The present work primarily compares the Grenville-Tilton correlation (1996) of the jet mixing time with CFD modeling results for three experimental tanks in an attempt to achieve fundamental understanding of the turbulent jet mixing and to establish the mixing indicators. These results are used in a quantitative way to validate the theoretical concept of using key turbulence parameters as mixing indicators. The analysis results demonstrate that the relationship between the jet Reynolds number and the final Taylor Reynolds number for a mixed condition is smooth for the combined data set of G-T data (1996) and ORNL test results (1994), a further indication that the initial conditions do not have a significant impact on the propagation of a scalar through the eddy regions of the tanks.

As discussed earlier, there are several important characteristics that all turbulent flows possess. These characteristics include flow fluctuations, rapid eddy diffusion, high levels of fluctuating vorticity, and eddy dissipation of kinetic energy. Figure 38 compares transient jet flow evolutions along the principal discharge direction inside Tank B with steady-state free jet results available in the literature. Flow conditions used in the figure are turbulent in terms of jet Reynolds number. In this case, the two-equation turbulence model, realizable k-ε (RKE) model, was applied to perform the calculations of jet flow into a stagnant liquid medium for a cylindrical tank.

As shown in Figs. 16 and 20, transient flow behaviors were monitored at the jet and remote regions. The results show that when tank liquid is initially quiescent, the velocity magnitudes increase monotonically from zero to a local maximum and then monotonically decrease during the early transient period. These results were considered questionable and in need of further investigation. Turbulence intensity also increases rapidly and then reaches a quasi-steady value after a transition period of flow fluctuation as shown in Fig. 39. It is noted that when comparing to the mixing time estimated by the G-T correlation, most local mixing takes place during this fluctuating period. Thus, the velocity fluctuations act to efficiently transport momentum, and possibly a second phase solid concentration, over the continuous fluid domain.

The second characteristic of turbulence is a high rate of diffusion due to the flow fluctuations. As shown in Fig. 40, this turbulent transport is significantly more effectively dissipative than molecular diffusion during the early stage of the transient period. In fact, it is common to model the transport due to the fluctuations by defining an effective diffusion coefficient called an eddy or apparent viscosity. While the velocity fluctuations are unpredictable, they possess a spatial structure. A turbulent flow consists of high levels of fluctuating vorticity. Instantaneous vortical motion, called eddies, are present in the flow. These eddies range in size from the largest geometric scales of the flow down to small scales where molecular diffusion dominates. The eddies are continuously evolving in time, and the superposition of their induced motions leads to the fluctuating time records as shown in Figs. 16 and 20.

Turbulent kinetic energy is passed down from the largest eddies to smallest through a process of energy cascade. At the smallest scales, the energy is eventually dissipated to heat by viscous effects. Thus, the last characteristic of turbulent flows is eddy dissipation of kinetic energy. To maintain turbulence, a constant supply of energy must be fed to the turbulent fluctuations at the largest scales from the mean motion.

As shown in Eq. (9), the information of the velocity fluctuations is used to estimate the length scale which provides information on eddy viscosity, ν_t. The constant ν_t with the derivative of the Reynolds stress in the average N-S equation is essentially a description of the length scale over which the energy quantity is diffused. This length is referred to as the mixing length, λ. The transient length scales corresponding to the energy dissipation at remote locations, point 6 and point 8, are shown in Fig. 33. The results show that eddies lose most of their energy at remote regions inside Tank B with about 100 mm dissipation scales, and the lost energy will result in local mixing. Thus, the eddy viscosity or diffusivity ν_t should involve the product of a turbulent mixing scale λ and a turbulent velocity scale.

While the turbulence parameters discussed show the ability to identify adequate transport of turbulence throughout the tank, it is convenient to combine them into another form, the Taylor Reynolds number. This allows a numerical criterion to be imposed on the measure with some support from the open literature (e.g, Dimotakis 2000). The results shown in Section 5.3 show not only that Re_T can be used as an effective measure, but also that it is not affected by the initial startup transient, thereby allowing the Grenville-Tilton data to be analyzed using the propagation of Re_T throughout the tank starting from stagnant conditions.

Finally, the mixing times were calculated for the ORNL test conditions by using the effective turbulent mixing indicator developed by using the G-T test results. Figure 42 compares the results of the ORNL test CFD calculations against test data. ORNL used a horizontal tank of 25,000 gallons with 10 ft diameter and 40 ft length. A horizontal nozzle with 1.94 in diameter is located near the tank bottom, and it is 10 ft away from the side tank wall. The benchmarking results demonstrated that the mixing indicator developed here, Re_T, predicts the mixing time well. As shown in the figure, a new correlation developed from recent SRNL experiments (Leishear et al. 2010) is compared with the G-T correlation (1996) along with the ORNL data.

Table 6. Test conditions of turbulent jets used in the present and literature

Authors	Jet diameter (mm)	Fluid	Reynolds number, Re_{jet}
Tank B (present)	26.1	Water	520,000
Kiser (1963)	9.525	Water	35,000
Post (1998)	10	Air	10,000

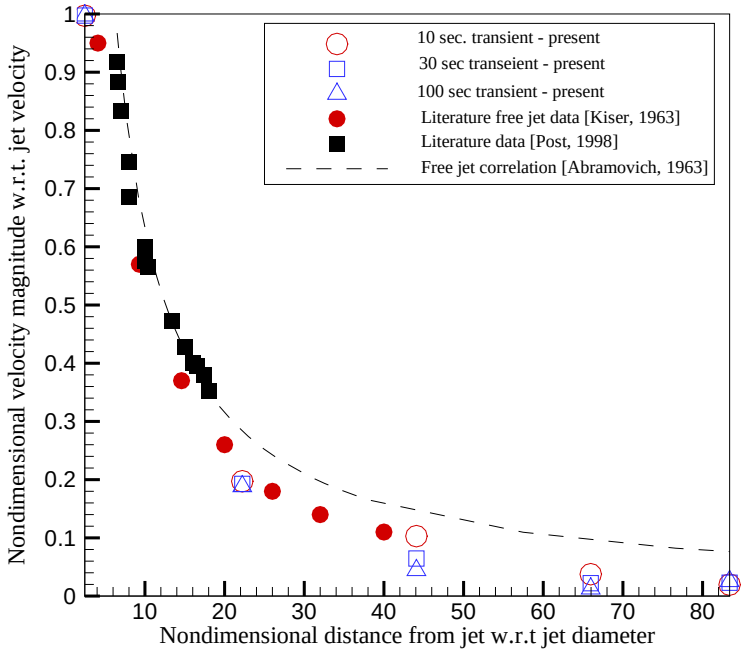

Figure 38. Comparison of transient jet flow evolutions with steady-state literature data along the principal discharge line inside Tank B (RKE model)

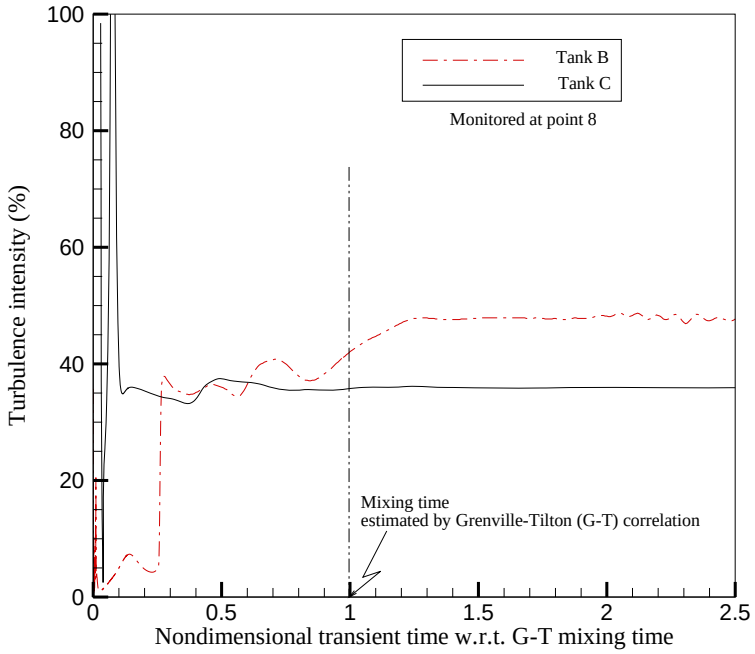

Figure 39. Transient turbulence intensity at remote monitoring point 8 far away from the principal discharge line inside Tank B and Tank C (RKE model)

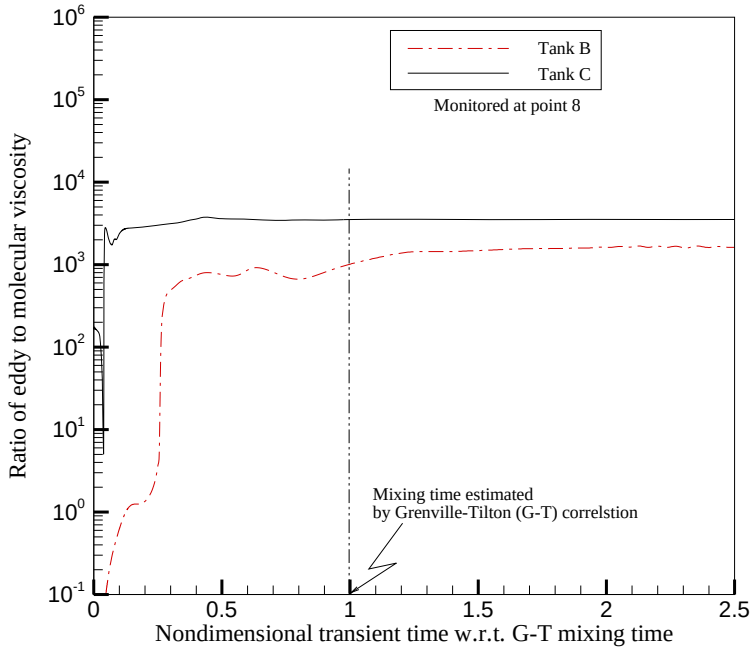

Figure 40. Transient turbulence eddy viscosity at remote monitoring point 8 far away from the principal discharge line inside Tank B and Tank C (RKE model)

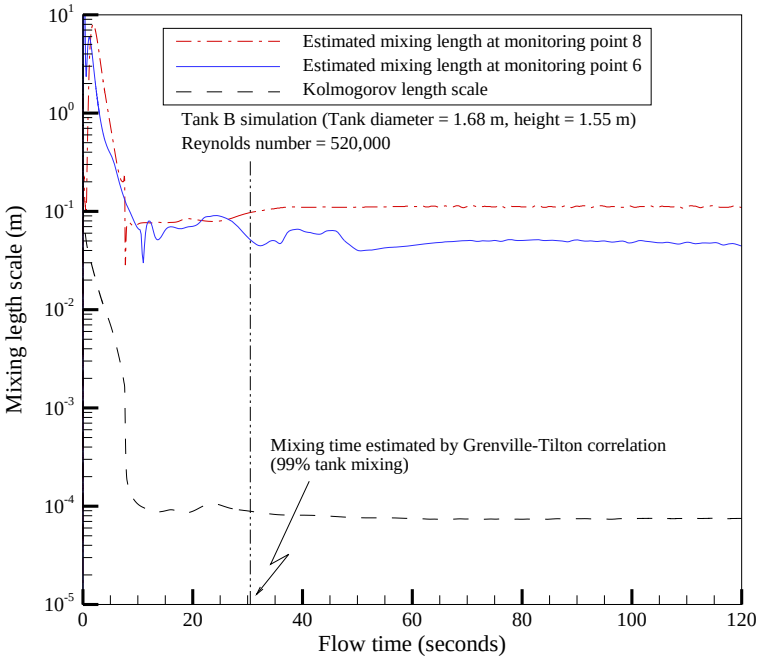

Figure 41. Transient turbulent mixing length scales at remote monitoring locations Point 6 and Point 8 far away from the principal discharge line inside Tank B (RKE model)

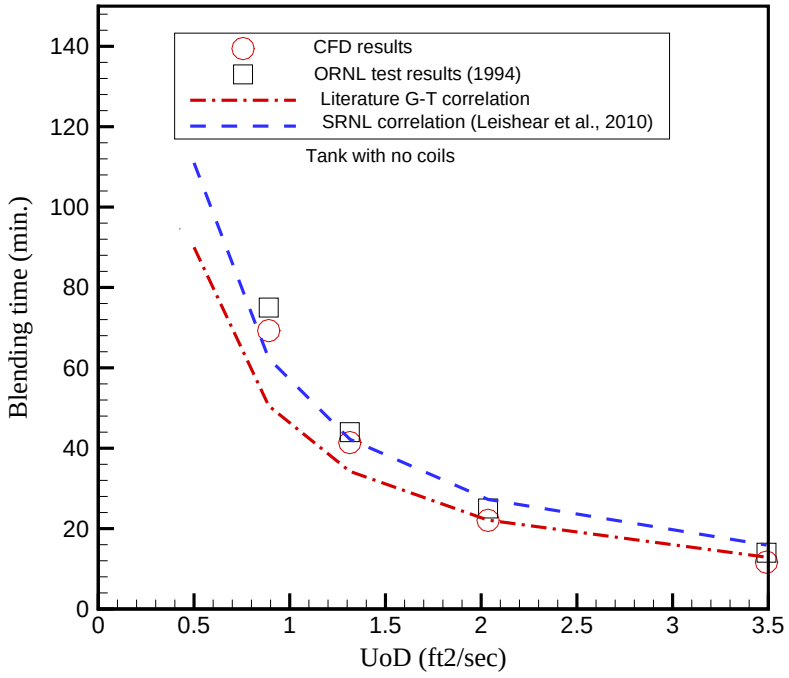

Figure 42. Quantitative comparison of mixing time between the CFD results and the literature test results

7.0 CONCLUSIONS AND SUMMARY

Turbulence parameters identified as potential indicators of mixing within a large tank were identified based on a two-equation turbulence closure model. The parameters selected were the turbulent kinetic energy, the turbulent kinetic energy dissipation rate, the turbulence eddy viscosity, and a combination of k and ε in the form of a Taylor Reynolds number. All were calculated for tank mixing geometries and conditions documented by Grenville and Tilton (1996) and compared against the results of their correlation for mixing time. The results obtained with CFD calculations were qualitatively similar to those observed by Grenville and Tilton.

The concept of using the identified mixing indicators to characterize a mixing time was shown to have promise by investigating a range of computational variations including grid sensitivity, time step sensitivity, tank geometries, jet dimensions, and Reynolds number. In all cases, qualitatively similar results were obtained between the calculated flow patterns and the Grenville-Tilton correlation.

Additional work showed that the initial conditions in the tank were not significant when evaluating the propagation of a scalar throughout the tank, and that starting from stagnant or fully developed conditions gave the same mixing time when using either the turbulence parameters proposed here or a separate concentration calculation of a contaminant species.

The main conclusions for the work are as follows:

- Theoretical concept of using key turbulence parameters as mixing indicators was established by using Grenville-Tilton correlation (1996, 1997) and ORNL data (1194) under several different conditions.
- The calculation results strongly indicate that convective flow patterns are primarily responsible for tank mixing, and the ratio of turbulent kinetic energy to dissipation rate at remote region controls the mixing time, depending on various jet flow conditions and tank geometry.
- The initial conditions do not have a significant impact on the propagation of a scalar through the eddy regions of the tanks or on the overall mixing time.
- The analysis results demonstrate that key turbulence parameters, energy dissipation rate and turbulent kinetic energy, provide good indicators of jet mixing.
- It is noted that when the tank is fully mixed, the ratio of the turbulence kinetic energy to dissipation rate, referred to as the Taylor length scale, is the size of the smallest eddies (1 mm order) which are responsible for local energy dissipation, and Taylor Reynolds number, the ratio of the Taylor-scale inertia to eddy-diffusion, reaches up to about 100 for high jet Reynolds number (~10^6). This is consistent with the literature results.
- The analysis results show that the Taylor length scale is closely related to the local loss of the turbulent energy production, which contributes to local mixing.

8.0 FUTURE WORK

Useful work remains to be accomplished to complete the analysis of mixing in single-phase systems by addressing the following issues:

1. Define the observable parameters to be used as mixing indicators. This will include as part of the definition an evaluation of how those indicators should be observed in the computational output.
2. Identify the most applicable models to calculate the local turbulence parameters and their combinations such as the Taylor Reynolds number.
3. Characterize the impact of using special near-wall models for flow near walls and internal obstructions.
4. Evaluate the impact of using a rotating pump or pumps as the mixing driver on the calculation of the indicators.
5. Apply the results of the single phase analysis to the suspension of sludge particles in a waste tank.

While all parameters affecting the calculation of turbulent flow behavior in a vessel will be considered potential variables, two of the most significant ones are grid density and Reynolds number. Both of these will be addressed as key parameters in the mixing evaluation.

Specific items of interest include

1. Guidelines for performing mixing calculations for a single-phase liquid system, observable parameters to calculate, and guidelines for interpreting those observable parameters to determine whether a tank is mixed.

2. Work to address mixing in two-phase systems.

9.0 REFERENCES

Abramovich, G. N. 1963 *The Theory of Turbulent Jets*, The MIT Press, Cambridge, MA.

Baldyga, J. & Bourne, J. R. 1984 "A Fluid Mechanical Approach To Turbulent Mixing and Chemical Reaction, Part III Computational and Experimental Results for the New Micromixing Model", *Chem. Eng. Commun*., Vol. 28, pp. 259-281.

Bradbury, L. J. S.,1965 "The Structure of a Self-Preserving Turbulent Plane Jet", *J. Fluid Mech*., Vol. 23, pp. 31-64.

Comte-Bellot, G. and Corrsin, S., 1966 "The Use of a Contraction to Improve the Isotropy of Grid-Generated Turbulence", *J. Fluid Mech*., vol. 25, pp. 657-682.

Davis, M. R. & Winarto, H. 1980 "Jet diffusion from a circular nozzle above a solid plane," *J. Fluid Mech*., Vol. 101, Part 1, pp. 201-221.

Dimotakis, P. E. 2000 "The mixing transition in turbulent flows," *J. Fluid Mech*., vol. 409, pp. 69-98.

Eckart, C. 1948 "An Analysis of the Stirring and Mixing Processes in Incompressible Fluids", *J. Mar. Research*, vol. 7, pp. 265 – 275.

Fischer, H. B. 1973 "Longitudinal Dispersion and Turbulent Mixing in Open-Channel Flow", *Annual Review of Fluid Mechanics*, Vol. 5, pp. 59-78.

Forstall, W., Jr. & Shapiro, A. H. 1950 "Momentum and Mass Transfer in Coaxial Gas Jets", *Journal of Applied Mechanics*, pp. 399-408, December.

Fossett, H. & Prosser, L. E. 1949 "The Application of Free Jets to the Mixing of Fluids in Bulk", *J. of Inst. of Mechanical Engineers*, Vol. 160, No. 2, pp. 224-232.

Fox, E. A. & Gex, V. E. 1956 "Single-phase Blending of Liquids", *A.I.Ch.E. Journal*, Vol. 2, No. 4, pp. 539-544.

Friehe, C. A., VanAtta, C W., and Gibson, C. H., 1972, "Jet Turbulence Dissiaption Rate Measurements and Correlations", AGARD Conference Proceedings Turbulent Shear Flows, No. 93, p. 18.

Grenville, R. K. 2009 Meeting in Philadelphia, Pa., to discuss computational approach and results. Participants: R. Grenville, R. Dimenna, S. Lee, D. Tamburello, M. Liu, A. Etchells, D. Rector, T. Michener, August 19.

Grenville, R. K. & Tilton, J. N. 1996 "A New Theory Improves the Correlation of Blend Time Data from Turbulent Jet Mixed Vessels", *Trans. Inst. of Chem. Eng*., Vol. 74, Part A., pp. 390-396.

Grenville, R. K. & Tilton, J. N. 1997 "Turbulent Flow or Flow as a Predictor of Blend Time in Turbulent Jet Mixed Vessels", Proceedings of 9th European Conf. on Mixing, pp. 67-74.

Hinze, J. O., 1975 *Turbulence, Second Edition*, McGraw-Hill, New York, p. 72.

Hussein, H. J., Capp, S. P., and George, W. K., 1994, "Velocity Measurements in a High-Reynolds-Number, Momentum-Conserving, Axisymmetric, Turbulent Jet", *J. Fluid Mech*., vol. 258, pp. 31-75.

Jones, W. P. and Launder, B. E., 1972, "The Prediction of Laminarization with a Two-Equation Model of Turbulence", *Int. J. of Heat Mass Transfer*, vol. 15, pp. 301-314, 1972.

Kays, W. M. & Crawford, M. E. 1980 *Convective Heat and Mass Transfer*, Second Edition, McGraw-Hill Book Company, New York.

Kim, J., Moin, P., and Moser, R., 1987 "Turbulent Statistics in Fully developed Channel Flow at Low Reynolds Number", *J. Fluid Mech*., vol. 177, pp. 133-166.

Kiser, K. M. 1963 "Material and Momentum Transport in Axisymmetric Turbulent Jets of Water", *A.I.Ch.E. Journal*, Vol. 9, No. 3, pp. 386-390.

Lane, A. G. C. & Rice, P. 1982 "An Investigation of Liquid Jet Mixing Employing an Inclined Side Entry Jet", *Inst. of Chemical Engineers*, Vol. 60, pp. 171-176.

Lee, S. Y., Dimenna, R. A., Leishear, R. A. & Stefanko, D. B. 2004 “Mixing in Large Scale Tanks Part I; Flow Modeling of Turbulent Mixing Jets”, HT-FED2004-5622, 2004 ASME Heat Transfer / Fluids Engineering Summer Conference, Charlotte, N. C., July 11-15.

Lee, S. Y., Dimenna, R. A., Leishear, R. A. & Stefanko, D. B. 2008 “Analysis of Turbulent Mixing Jets in a Large Scale Tank”, *ASME Journal of Fluids Engineering*, Volume 130, Number 1, pp. 011104.

Leishear, R. A., Poirier, M. R., and Fowley, M. D. 2010 “SDI Blend and Feed Blending Study: Tank 50H Scale Modeling for Blending Pump Design Phase 1, Savannah River National Laboratory, SRNL-STI-2010-00054.

Miller, P. L. 1991 “Mixing in High Schmidt Number Turbulent Jets”, PhD Thesis, California Inst. of Technology.

Okita, N. & Oyama, Y. 1963 “Mixing Characteristics in Jet Mixing”, *Chemical Engineering*, The Society of Chemical Engineers, Japan, Vol. 1, No. 1, pp. 92-101.

Panchapakesan, N. R. and Lumley, J. L. 1993 “Turbulence Measurements in Axisymmetric Jets of Air and Helium, Part 1. Air Jet”, *J. of Fluid Mech.*, Vol. 246, pp. 197-223.

Patwardhan, A. W. & Joshi, J. B. 1999 ”Relation between Flow Pattern and Blending in Stirred Tanks,” *Ind. Eng. Chem. Res*., 38, pp. 3131-3143.

Patwardhan, A. W., Pandit, A. B. & Joshi, J. B. 2003 “The role of convection and turbulent dispersion in blending,” *Chem. Eng. Sci*. 58, pp. 2951-2962.

Perona, J. J., Hylton, T. D., Youngblood, E. L. & Cummins, R. L. 1994 “Jet Mixing Long Horizontal Storage Tanks,” ORNL/TM-12876, Oak Ridge National Laboratory.

Perona, J. J., Hylton, T. D., Youngblood, E. L. & Cummins, R. L. 1998 “Jet Mixing of Liquids in Long Horizontal Cylindrical Tanks”, *Ind. Eng. Res*., Vol. 37, pp. 1478-1482.

Post, S. 1998 “A Computational and Experimental Study of Near-Field Entrainment in Steady Gas Jets,” MSME thesis, Purdue University.

Ricou, F. P. & Spalding, D. B. 1961 “Measurements of Entrainment by Axisymmetrical Turbulent Jets”, *J. Fluid Mech.*, Vol. 11, pp. 21-32.

Rushton, J. H. 1980 “The Axial Velocity of a Submerged Axially Symmetrical Fluid Jet”, *AIChE Journal*, Vol. 26, No. 6, pp. 1038.

Simon, M. & Fonade, C. 1993 “Experimental Study of Mixing Performances Using Steady and Unsteady Jets,” *The Canadian J. of Chem. Eng*., Vol. 71.

Spalding, D. B. 1971 “Mixing and Chemical Reaction in Steady Confined Turbulent Flames”, 13th International Symposium on Combustion, 649-657.

Tennekes, H. & Lumley, J. L. 1972 *A First Course in Turbulence*, The MIT Press, Cambridge.

APPENDIX

The flow of fluid through a pipe of uniform (circular) cross-section is known as Hagen-Poiseuille flow. The Hagen-Poiseuille flow is an exact solution of the Navier-Stokes equations in fluid mechanics. The equations governing the Hagen-Poiseuille flow can be derived from the Navier-Stokes equation in cylindrical coordinates by making the following set of assumptions:

- The flow is steady.
- The radial and swirl components of the fluid velocity are zero ($u_r = u_\theta = 0$).
- The flow is axisymmetric and fully developed.

Then the second of the three Navier-Stokes momentum equations and the continuity equation are identically satisfied. The first momentum equation reduces to, i.e., the pressure p is a function of the axial coordinate z only. The third momentum equation reduces to:

$$\mu \frac{1}{r}\frac{\partial}{\partial r}\left\{r\left(\frac{\partial u}{\partial r}\right)\right\} = \left(\frac{dp}{dz}\right) \tag{A1}$$

The solution is

$$u_z = \left(\frac{1}{4\mu}\right)\left(\frac{dp}{dz}\right)r^2 + C_1 \ln r + C_2 \tag{A2}$$

Since u_z needs to be finite at $r = 0$, $c_1 = 0$. The no slip boundary condition at the pipe wall requires that $u_z = 0$ at $r = R$ (radius of the pipe), which yields

$$C_2 = -\left(\frac{1}{4\mu}\right)\left(\frac{dp}{dz}\right)R^2 \tag{A3}$$

$$u_z = -\left(\frac{R^2}{4\mu}\right)\left(\frac{dp}{dz}\right)\left\{1 - \left(\frac{r}{R}\right)^2\right\} \tag{A4}$$

$$Q = \int_0^R u_z dA = -\left\{\left(\frac{\pi R^4}{8\mu}\right)\left(\frac{dp}{dz}\right)\right\} \tag{A5}$$

$$\mu = -\left\{\left(\frac{\pi R^4}{8Q}\right)\left(\frac{dp}{dz}\right)\right\} \approx \left(\frac{\pi R^4 \Delta p}{8QL}\right) = \left(\frac{\pi R^4}{8Q}\right)\left(\frac{\Delta p}{L}\right) \tag{A6}$$

This corresponds to laminar flow regime. So, it can be extended to the application of turbulent flow regime since average pressure gradients for both of the flow regimes are closely related to the viscosity for given flow conditions.

$$\mu_t \approx \left\{\left(\frac{\pi R^4}{8Q}\right)\left(\frac{\Delta p}{L}\right)_t\right\} \tag{A7}$$

The power P for flow rate Q is

$$P \approx Q\Delta p \tag{A8}$$

In this case, energy dissipation rate per unit volume, ε_v, can be quantified.

$$\varepsilon_v \approx \left(\frac{Q\Delta p}{V}\right) = \left(\frac{Q}{\pi R^2}\right)\left(\frac{\Delta p}{L}\right)_t \quad \text{(A9)}$$

Pressure gradient for Eq. (A9) can be expressed in terms of turbulent viscosity (μ_t) from Eq. (A7).

$$\varepsilon_v \approx 32\left(\frac{\overline{u}}{D}\right)^2 \mu_t \quad \text{(A10)}$$

Turbulent energy dissipation rate per unit mass, ε, is associated with turbulent eddy viscosity. That is,

$$\varepsilon = \frac{1}{\rho}\varepsilon_v = 32\left(\frac{u}{D}\right)^2 \nu_t \quad \text{(A11)}$$